

Airborne flux measurements of Biogenic Volatile Organic Compounds over California

P. K. Misztal^{1,2}, T. Karl^{2,3}, R. Weber¹, H. H. Jonsson⁴, A. B. Guenther^{2,5}, and A. H. Goldstein¹

[1]{University of California at Berkeley, Berkeley, California, USA}

[2]{National Center for Atmospheric Research, Boulder, Colorado, USA}

[3]{now at: Institute for Meteorology and Geophysics, University of Innsbruck, Innsbruck, Austria}

[4]{Center for Interdisciplinary Remotely-Piloted Aircraft Studies, Monterey, CA, USA}

[5]{now at: Atmospheric Sciences and Global Change Division, Pacific Northwest National Laboratory, Richland, WA, USA}

Correspondence to: P. K. Misztal (pkm@berkeley.edu)

Abstract

Biogenic Volatile Organic Compound (BVOC) fluxes were measured onboard the CIRPAS Twin Otter aircraft as part of the California Airborne BVOC Emission Research in Natural Ecosystem Transects (CABERNET) campaign during June 2011. The airborne virtual disjunct eddy covariance (AvDEC) approach used measurements from a Proton Transfer Reaction Mass Spectrometer (PTR-MS) and a wind radome probe to directly determine fluxes of isoprene, MVK+MAC, methanol, monoterpenes, and MBO over 7,400 km of flight paths focusing on areas of California predicted to have the largest emissions of isoprene. The Fast Fourier Transform (FFT) approach was used to calculate fluxes over long transects of more than 15 km, most commonly between 50 and 150 km. The Continuous Wavelet Transformation (CWT) approach was used over the same transects to also calculate “instantaneous” fluxes with localization of both frequency and time independent of non-stationarities. Vertical flux divergence is expected for all atmospheric species, but a major contribution for isoprene is due to its relatively short atmospheric lifetime. Vertical flux divergence was measured directly using “racetrack” profiles at multiple altitudes and was

1 found to be linear. The flux divergence correction was in the range 5% to 30% (surface flux
2 higher than flight level flux) depending on the ratio of aircraft altitude to PBL height (z/z_i).
3 Fluxes were generally measured by flying consistently at 400 m \pm 50 m (a.g.l.) altitude, and
4 extrapolated to the surface according to the determined flux divergence. The wavelet-derived
5 surface fluxes of isoprene averaged to 2 km spatial resolution showed good correspondence
6 to Basal Emission Factor (BEF) landcover datasets used to drive biogenic VOC (BVOC)
7 emission models. The surface flux of isoprene was close to zero over Central Valley crops
8 and desert shrublands, but was very high (up to 15 mg m⁻² h⁻¹) above oak woodlands, with
9 clear dependence of emissions on temperature and oak density. Isoprene concentrations of up
10 to 8 ppb were observed at aircraft height on the hottest days and over the dominant source
11 regions.

12 While isoprene emissions from agricultural crop regions, shrublands, and coniferous forests
13 were extremely low, high concentrations of methanol and monoterpenes were found above
14 some of these regions.

15 These observations demonstrate the ability to measure fluxes from specific sources by eddy
16 covariance from an aircraft, and suggest the utility of measurements using fast response
17 chemical sensors to constrain emission inventories and map out source distributions for a
18 much broader array of trace gases than was observed in this study.

19 This paper reports the first regional direct eddy covariance fluxes of isoprene. The emissions
20 of VOCs measured from aircraft with 2 km spatial resolution can quantify the distribution of
21 major sources providing the observations required for testing statewide emission inventories
22 of these important trace gases. These measurements will be used in a future study to assess
23 BVOC emission models and their driving variable datasets.

24

25 **1 Introduction**

26 Volatile Organic Compounds (VOCs) play important roles in atmospheric chemistry such as
27 fueling tropospheric ozone production, forming secondary organic aerosols, and acting as
28 important radical sinks in regions near sources. The global annual source strength of gas-
29 phase biogenic volatile organic compounds (BVOC) is around 1 Pg (10¹⁵ g) (Guenther et al.,
30 2012). One half of these mass emissions (500 Tg) is constituted by a single highly reactive
31 hemiterpene, isoprene (2-methyl-1,3-butadiene). The other half is represented by hundreds to

1 thousands of compounds which span the atmospheric lifetime ranges from a few seconds
2 (e.g. sesquiterpenes) to months (e.g. benzene), and are actively exchanged in both directions
3 (emission and deposition) between the biosphere and atmosphere (Park et al., 2013).
4 Currently, BVOC measurements (mostly of emission) have been reported at ecosystem scales
5 primarily from fixed tower sites which offer very good temporal resolution, but lack spatial
6 resolution across the broader landscape that is critical for understanding regional
7 photochemistry.

8 Since the discovery of substantial isoprene emissions from forested regions (Rasmussen,
9 1970), and subsequent progress in understanding isoprene biochemistry (Loreto and Sharkey,
10 1990), much research has been conducted to understand the emissions of isoprene and the
11 factors that drive them at the leaf level, including in California (Arey et al., 1991; Arey et al.,
12 1995; Baker et al., 1999; Karlik and Winer, 2001; Kurpius and Goldstein, 2003; Goldstein
13 and Schade, 2000; Schade et al., 1999; Schade et al., 2000; Schade and Goldstein, 2001;
14 Winer et al., 1992). This work has led to BVOC emission models such as Biogenic Emission
15 Inventory System (BEIS) (Pierce et al., 1998), Model of Emissions of Gases and Aerosols
16 from Nature (MEGAN) (Guenther et al., 2012) and Biogenic Emission Inventory Geographic
17 Information System (BEIGIS) (Scott and Benjamin, 2003) that are driven by information
18 about weather conditions, plant distributions, leaf area, and the temperature and light
19 response of isoprene emissions from plants. There have been isoprene flux measurements at
20 the canopy scale in a variety of locations worldwide: Northwestern U.S. oak savanna (Lamb
21 et al., 1986), Northeastern US mixed forest (Goldstein et al., 1998), North Central US mixed
22 forest (Westberg et al., 2001; Apel et al., 2002), Amazonian tropical forests (Rinne et al.,
23 2002; Kuhn et al., 2002), Central Africa rainforest (Serca et al., 2001), Borneo rainforest
24 (Langford et al., 2010), etc. However, in California, no ecosystem scale fluxes have ever been
25 reported for an oak dominated ecosystem that could be used to verify the modeled statewide
26 isoprene emission inventory.

27 A California BVOC model called BEIGIS (Scott and Benjamin, 2003) predicts significant
28 emissions of isoprene from oak woodlands distributed throughout the foothills of the Coast
29 Range and the Sierra Nevada mountains (Figure 1a). However, with the exception of a single
30 site in a pine plantation (Schade et al., 1999; Schade et al., 2000; Goldstein and Schade,
31 2000; Schade and Goldstein, 2001), and measurements in a few crops (Karl et al., 2008;
32 Fares et al., 2011; Fares et al., 2012; Park et al., 2013), there have been no measurements of

1 BVOC fluxes from California landscapes at a larger spatial scale than individual leaves and
2 branches. The goal of our work was to measure the distribution of isoprene flux across the
3 oak woodland areas of California in order to test and improve the landscape-scale emission
4 models that are used for regional air quality assessments. The motivation for conducting this
5 regional flux study in California was driven by: 1) the need for spatially resolved data on
6 BVOC emissions from oak woodlands which have a large impact on regional ozone
7 concentrations, and 2) our lack of information on how BVOC emissions respond to variations
8 in landcover (plant functional type distributions, LAI, etc).

9 California is a region where these observations are particularly needed because of its varied
10 landscape, with BVOC emissions from biogenic areas dominated by Oaks (~7% of land
11 area), and with anthropogenic VOC emissions from the activity of ~35 million people living
12 in the state. Furthermore, the accuracy of isoprene emission estimates is important for
13 regional simulations of ozone production.

14 Airborne Eddy Covariance (AEC) is an established technique which has been used
15 extensively in the last several decades to measure fluxes (e.g. of energy, ozone, carbon
16 dioxide, etc.) directly using an aircraft (e.g. Lenschow et al., 1981; Desjardins et al., 1992;
17 Pattey et al., 2002; Metzger et al., 2013). The first successful implementation of AEC for
18 VOC was by Karl et al. (2009) over Mexico using a C130 aircraft.

19 We begin this paper (Sect. 2) by describing the methodology used and the context of the
20 CABERNET airborne campaign including the study region, climatology, flight-track
21 planning, aircraft, instrumentation, and the airborne flux methodologies. We then present
22 results and discussion (Sect. 3) of the BVOC concentration and isoprene flux measurements
23 focused on transects over areas expected to dominate BVOC emissions in California. Stacked
24 “racetrack” profiles which were used for testing the flux methodology and derivation of flux
25 divergence terms were recently described in a separate paper (Karl et al., 2013) where we
26 demonstrated that our PTR-MS configuration in CABERNET was appropriate for measuring
27 isoprene fluxes. Finally, we report the first observed regional spatial distribution of airborne
28 fluxes and emission factors and demonstrate that they match well the emission factors from
29 landcovers estimated using a California Air Resources Board implementation of the MEGAN
30 model. The comparison of observed fluxes with emissions models will be more thoroughly

1 explored in a separate paper focused on improving landcover databases and accuracy of VOC
2 inventories in California (Misztal et al., 2014).

3

4 **2 Methodology**

5 **2.1 Study region**

6 Oaks are the main source of isoprene in California and they grow dominantly in certain
7 elevations (400-800 m) along the foothills encompassing the Central Valley and along the
8 Coastal Range Mountains. These specific locations, relatively constant elevations, and high
9 emission rates make oaks an ideal subject for flux observations from aircraft. Using the
10 USGS National Gap Analysis Program (GAP) landcover database, we planned our survey
11 flights (to infer surface fluxes from flux measurements over long transects at constant
12 altitude) and racetrack flights at several levels (vertical profiles to characterize flux
13 divergence) over more or less homogeneous oak woodlands consisting of the Blue Oak
14 Woodlands (BOW), Valley Oak Woodlands (VOW) and Coastal Oak Woodlands (COW).
15 The total percentage of the sum of their primary, secondary and tertiary levels was used to
16 map out the most homogeneous areas where oaks are the only or the dominating tree species
17 (see Sect. 2.3 on flight track planning). Despite this biological homogeneity the oaks have
18 highly irregular distribution patterns characterized by varying spatial densities.
19 Supplementary Fig. S1 shows a typical oak ecosystem as seen from the Twin Otter flying
20 over Tonzi Ranch tower, where ground flux measurements of isoprene were simultaneously
21 performed for comparison with the aircraft observations (see Sect. 3.2.2). Apart from
22 relatively homogeneous (in terms of the species) oak woodlands mostly in the foothill bands,
23 further away there are transition areas with coniferous regions where, according to the GAP
24 database, the oaks grade in to Blue Oak – Ponderosa Pine (BOP) habitats and/or Montane
25 Hardwood-Conifer (MHC), and/or Montane Hardwood (MHW). These areas are represented
26 in Figure 1b.

27 **2.2 Climatology during field campaign**

28 Environmental context is important to take into account when analyzing measured BVOC
29 fluxes because the history of temperature and photosynthetically active radiation (PAR) is the

1 main driver of potential vegetative emissions (Sharkey et al., 1999; Fuentes and Wang,
2 1999), and seasonal variability in climate is known to affect gross ecosystem production in
3 this region (Goldstein et al., 2000). The climatological conditions in California in June 2011
4 were relatively colder than in June of the previous year. The preceding month and the first
5 week of June 2011 were particularly cold followed by gradual increase in the temperature
6 throughout the campaign with particularly hot sunny weather on the final flight of the
7 campaign. Along with the warming, the environment was becoming dryer.

8 **2.3 Flight track planning**

9 The CABERNET airborne campaign took place in June 2011. The paths of the research
10 survey flights and “racetrack” gradient flights are portrayed over the BEIGIS isoprene
11 emission factor map (Figure 1a) and California map of oak woodland distribution (Figure
12 1b). Weather forecasting was used to ensure that all the flights were conducted on cloudless
13 days, and where possible for the mean wind direction to be perpendicular to the flight paths.
14 A test flight on June 1st was performed over the ocean to calibrate the sensors using pitch and
15 yaw maneuvers, according to Lenschow (1986). These were used for dynamic upwash
16 correction and to test the accuracy of coefficients for wind vector transformations to ensure
17 the vertical wind speed is not affected by aircraft motion. More detailed information on these
18 maneuvers made during CABERNET can be found in Karl et al. (2013).

19 The true air speed (TAS) was kept as constant as possible on all the flights. For the entire
20 campaign the TAS ranged from around 52 to 67 m/s with an average of 58 m/s, and a
21 standard deviation of 2.3 m/s. The measured air temperature at aircraft altitude ranged from
22 19.4 to 25.9 °C (mean: 22.5 °C, s.d.: 1.28 °C) while the temperature at 2 m above the surface
23 (WRF model) was wider in range (from 10.9 to 34.8 °C) and higher by 3.6 °C average
24 temperature.

25 The available forty hours of flight time was divided into eight research flights (RF) which
26 were carried out for approximately 4-5 hours each during the mid-day. The individual flown
27 tracks are described in sections 2.3.1 to 2.3.8.

28 Further information specific to each research flight (RF) is summarized in Table 1 and
29 described in Supplementary Information.

30

1 **2.4 Aircraft**

2 A two-engine UV-18A Twin Otter (the military version of model Series 300) research
3 aircraft was operated by the Center for Interdisciplinary Remote Piloted Aircraft Study
4 (CIRPAS) of the Naval Postgraduate School out of the airport located in Marina, CA near
5 Monterey, CA. The aircraft is equipped with micrometeorological sensors and is capable of
6 eddy flux measurements (Karl et al., 2013). Air was drawn from a 3-inch (76 mm) isokinetic
7 pipe inlet extending above the nose of the plane, resulting in a flow speed inside the tube of
8 about 10% of the aircraft speed ($\sim 60 \text{ m s}^{-1}$). The vertical wind speed in the airplane
9 coordinate system was measured by a five-hole radome probe with 33° half-angles at the nose
10 of the aircraft. The vertical wind speed with respect to the earth is obtained from this
11 measured vertical wind speed corrected for airplane motions measured by an inertial
12 reference unit. The measured vertical wind speed is affected by the aircraft movement and
13 flow distortion at the nose, but this affect can be minimized by applying corrections based on
14 “Lenschow maneuvers” (Lenschow, 1986). More detailed descriptions of this particular
15 aircraft can be found elsewhere (Hegg et al., 2005; Reid et al., 2001).

16 The aircraft payload is relatively large allowing for an extensive set of instrumentation and
17 between 1 and 3 research crew on board. The list of instrumentation included: 1) NCAR’s
18 airborne PTR-MS for VOC fluxes (Karl et al., 2009); 2) NCAR’s custom-built adsorbent-
19 cartridge automatic sampler for GC-MS VOC speciation and validation of contributions to
20 m/z measured by the PTR-MS; 3) a Picarro (1301-m) 2 Hz methane/CO₂ analyzer; 4) a slow
21 ozone analyzer (2B Tech) and dry chemo-luminescent fast-ozone sensor (NOAA); and 5) a
22 water-based Condensation Particle Counter (CPC, TSI Inc.).

23 The VOC cartridge sampler containing 8 adsorbent tubes was manually activated during the
24 flight and was recorded by a datalogger analog input to mark the timing of each sample,
25 which was drawn automatically through the cartridge for 8 min at a constant flow of 335
26 standard cubic centimeters per minute (sccm). In addition, one tube served as a blank for each
27 flight and one tube was kept open inside the cabin for passive absorption of VOCs present in
28 the cabin air to help in the identification of potential tube leaks.

2.5 Proton Transfer Reaction Mass Spectrometry (PTR-MS)

The Proton Transfer Reaction Mass Spectrometer (PTR-MS) can measure concentrations of VOC in a high frequency (10 Hz) virtual disjunct mode (Karl et al., 2002). Unlike a disjunct sampler which rapidly grabs a sample periodically, a PTR-MS instrument can be regarded as a virtual disjunct sampler where the ambient air is sampled continuously but m/z are analyzed sequentially by the quadrupole detector, creating a disjunct dataset with high frequency data (e.g. 10 Hz) separated by a relatively longer gap (e.g. 0.5 s). Thus, the 10-Hz disjunct sampling corresponded to 0.1-s dwell time and approximately 2 samples/s.

The instrument deployed in CABERNET was NCAR's high sensitivity PTR-MS (Karl et al., 2009). Its internal vacuum inlet system was specifically redesigned to enable stable operation across a wide range of altitudes and to ensure internal lag-time of less than 100 ms. The instrument operation and routine were kept consistently constant for each flight. Current FAA regulations do not allow for the instrumentation to be running overnight, requiring specific steps to achieve stable instrument operation quickly after an instrument start-up. A flight-optimized vacuum system and internal capillary components result in fast transfer time from the inlet to the drift tube and independence of ambient pressure variations on the drift-tube pressure at high altitudes. The valves between the water reservoir and the ion source reduce the time to achieve ion source stability and low oxygen ion levels in the drift tube. Approximately three hours before the take-off the instrument was powered up, and approximately 1 hour before the take-off, if the O_2^+ signal went below 6% of the primary ions, a secondary electron multiplier (SEM) and ion source check with optimization was followed by a dynamic calibration using two VOC standards (Apel-Riemer), one high concentration (available during pre-flight) containing low-fragmenting compounds for daily sensitivity curves (i.e. benzene (1.11 ppm), toluene (1.07 ppm), xylenes (4.22 ppm), trimethylbenzene (1.94 ppm), dichlorobenzene (2.61 ppm), and trichlorobenzene (1.14 ppm)) diluted with VOC-free air and another low-concentration standard containing isoprene (10.0 ppb) (also available in-flight) which was also used as a back-flushing gas during the take-offs and touch-downs to prevent the exhaust plumes from contaminating the inlet. Zeros were measured using three different sources: Pt-catalyzed ambient air; ultra-pure compressed air (Air Liquide); ambient air at the top of the saw-tooth sounding well above the PBL height. The calibrated normalized sensitivities for calibrated VOCs experienced day-to-day variabilities of less than 30%. The average sensitivity for isoprene was 15.1 normalized

1 counts per second per ppbv (ncps ppbv⁻¹) as a sum of m/z 69 (13.4 ncps ppbv⁻¹) and m/z 41
2 (2.2 ncps ppbv⁻¹). The m/z 41 ion was used to assess the stability of isoprene fragmentation
3 but only m/z 69 was used in the calculation of concentrations. These high sensitivities
4 ensured low detection limits (e.g. <10 pptv for isoprene at 1-km averaging (~17 s)). The
5 primary ion count rates monitored at m/z 21 were around $2.0 \cdot 10^7$ counts per second (cps)
6 ($\pm 20\%$) so the absolute sensitivities were approximately 20 times higher than the normalized
7 sensitivities (i.e. ~300 cps ppbv⁻¹ for isoprene). The sensitivities for compounds not present in
8 the standard were approximated for each day from combining sensitivity curves of the daily
9 calibrations with sensitivity curves from post-campaign calibrations using several different
10 standards at a range of humidities. The accuracy of sensitivities was estimated at $\pm 10\%$ for
11 direct calibration (5% standard certification + 5% from dilution) and $\pm 30\%$ for the approach
12 combining post-campaign calibrations. The settings, sensitivities and further methodological
13 remarks are included in Supplementary Table S1.

14 **2.6 Airborne eddy covariance (AEC)**

15 The preferred micrometeorological method for measuring trace gas fluxes in the turbulent
16 boundary layer is eddy covariance (EC). This approach is a direct measurement of the
17 fluctuating vertical wind velocity and trace gas concentration. The flux is determined from
18 the mean covariance between vertical wind velocity (w) and concentration (c) fluctuations
19 and can be expressed as

$$20 \quad F = \overline{w'c'} \quad (1)$$

21
22 where w' is the difference between the instantaneous and mean vertical wind speed and c' is
23 the difference between the instantaneous and mean trace gas concentration. Here we use $\overline{w'c'}$
24 to represent the time average of the product of these two variables. The major components of
25 an EC flux system are: 1) a system that measures vertical wind speed with a fast (typically
26 <100 ms) response time; 2) an instrument that measures the targeted atmospheric constituent
27 with a fast response time; and 3) a system to receive and store the data (e.g. datalogger or
28 computer). Instruments with slower (> 100 ms) response times can be used to measure the
29 flux associated with lower frequencies but may underestimate the total flux depending on the
30 frequency of the transporting eddies. In some cases this may result in an acceptable error

1 while in other cases an attempt can be made to account for the loss of flux due to inadequate
2 sensor response (Moore, 1986; Rowe et al., 2011). One way for estimating high frequency
3 correction involves using another scalar that is measured with a fast response sensor and then
4 estimating the reduction in flux that results if a digital filter is used to simulate response time
5 of the slower instrument.

6 EC is used extensively to measure sensible and latent heat fluxes, and has recently been used
7 for networks dedicated to quantifying carbon dioxide fluxes from various landscapes
8 (Baldocchi, 2003). Commercial fast response instruments are available for some compounds
9 (e.g. CO₂, H₂O, CH₄) and others can be constructed for additional chemical species. EC is
10 generally preferred as the most direct flux measurement method which does not require
11 parameterizations. Fluxes of VOC with short lifetimes can be estimated from flux divergence
12 measurements (Lenschow et al., 1980).

13 Wyngaard and Brost (1984) proposed that the surface fluxes could also be estimated from
14 measurements of vertical concentration profiles in the daytime convective boundary layer
15 (CBL) that lies above the surface layer and can extend up to several km. This method
16 assumes that the mean vertical gradient of a conserved species in the CBL is determined by
17 the depth of the CBL (z_i), the convective velocity scale (w^*), and the fluxes at the bottom and
18 the top of the CBL. We used vertical profiles of temperature and humidity measured during
19 “saw-tooth soundings” (steep climbs through PBL and part of the free troposphere [e.g. up to
20 3 km] at a constant angle followed by the similarly steep descent) to directly characterize z_i
21 and measured sensible heat fluxes to quantify w^* . The CBL gradient-flux technique assumes
22 that boundary layer mixing is dominated by convective turbulence and that boundary layer
23 conditions evolve slowly compared to the convective turnover time of about 7 minutes. The
24 results are not affected by vertically homogeneous horizontal advection or time dependence
25 in the mean concentration and the method can account for entrainment.

26 A time scale at a fixed point in the PBL can be related to a length scale by multiplying the
27 time scale by the average wind speed, as long as the “frozen turbulence” hypothesis known as
28 Taylor’s hypothesis (e.g. Panofsky and Dutton, 1984) is fulfilled. This hypothesis enables
29 approximate conversion from temporal to spatial statistics. Since aircraft can fly an order of
30 magnitude faster than the mean wind, Taylor’s hypothesis is more easily fulfilled, so the
31 length scales can be calculated by multiplying the measured time scale by the true airspeed.

1 Area source emission was measured using the airborne eddy covariance technique. Eddy
2 covariance was used to directly measure fluxes of predetermined compounds. Because
3 quadrupole systems analyze mass to charge ratios sequentially, only a small number of
4 compounds can be selected for inclusion into the flux mode to keep the disjunct gap
5 relatively small. The number of masses ranged from three to six during eight research flights.
6 As the project was focused on California vegetation and in particular oak woodlands,
7 isoprene (m/z 69) was measured on all eight research flights, MVK+MACR (m/z 71) and
8 methanol (m/z 33) on seven flights. Other VOCs measured on a smaller number of flights
9 included monoterpenes (m/z 81, 137), MBO (m/z 87), acetaldehyde (m/z 45), benzene (m/z
10 79), toluene (m/z 93), and C8-aromatics (m/z 107). Spatially resolved eddy covariance fluxes
11 were calculated using Wavelet Analysis (Mauder et al., 2007) along flight tracks through the
12 convective layer. Since the majority of flights were conducted in the lower part of the mixed
13 layer and the upper part of the surface layer (typically 100-200 m deep based on 10% of the
14 measured PBL depth), we estimate the horizontal spatial resolution based on the blending
15 height (e.g. Claussen, 1990) using the surface layer scaling and the parameterizations for the
16 mixed layer scaling (Karl et al., 2013).

17 2.6.1 Airborne virtual Disjunct Eddy Covariance (AvDEC)

18 The difference between virtual and conventional disjunct eddy covariance is that sampling
19 flow is continuous but the dataset becomes disjunct because the quadrupole detector cycles
20 through the m/z sequentially, producing regular gaps between high-frequency data points. For
21 the small number of m/z scanned by the PTR-MS detector, AvDEC measurements are nearly
22 equivalent to continuous AEC. In order to minimize the disjunct error the number of samples
23 collected per integral scale should significantly exceed 1 and the effective duration of the
24 sample period should be maximized. This can be achieved by limiting the number of m/z in
25 the duty cycle and keeping the integration time long. We kept the number of VOC-related m/z
26 between 3 and 6 at 0.1 s dwell time. In addition, on each flight, we monitored three control
27 masses: hydronium ions (m/z 21), oxygen ions (m/z 32), and water vapor (m/z 37) at 0.1, 0.05,
28 and 0.05 s, respectively, so the total duty-cycle length varied from 0.5 to 0.8 s between
29 different flights which resulted in a sampling rate of 1.25 to 2 samples/s.

1 2.6.2 Fast Fourier Transform (FFT)

2 Fast Fourier Transform (FFT) is the conventional method to compute airborne flux. This
3 method provides a single value for a given segment of flight, which limits the spatial
4 resolution. The optimal stretch for flux calculation would be a sufficiently long pass to
5 capture the optimal range of frequency distribution, but not so long that the turbulent
6 structures are affected by diurnal effects. Therefore, resolution finer than 10 km would be
7 challenging and uncertain using the FFT approach. Another challenge in this method is that it
8 is affected by non-stationarities (e.g. related to heterogeneities). However, as an independent
9 method it can be very useful for comparison with fluxes obtained from wavelet analysis (see
10 Sect. 2.6.3).

11 2.6.3 Continuous Wavelet Transform (CWT)

12 Wavelet analysis, originally demonstrated to work with seismological data, has recently
13 become increasingly popular in environmental and biological applications. Examples can be
14 found in the analysis of the turbulent structures (Thomas and Foken, 2005; Mauder et al.,
15 2007; Steiner et al., 2011; Metzger et al., 2013), and analysis of environmental processes at
16 multiple scales (Stoy et al., 2009; Vargas et al., 2010).

17 The mathematic principle for the one-dimensional wavelet transform of a given signal $f(t)$ can
18 be presented as:

$$19 T_p(a,b) = \int_{-\infty}^{+\infty} f(t) \overline{\Psi_{p,a,b}(t)} dt, \quad (4)$$

20

21 where $T_p(a,b)$ are wavelet coefficients and $\Psi_{p,a,b}(t)$ is the wavelet function given by:

$$22 \Psi_{p,a,b} = \frac{1}{a^p} \Psi\left(\frac{t-b}{a}\right), \quad (5)$$

23

24 where $\Psi((t - b)/a)$ is termed "the mother wavelet", of which shape and locations are
25 determined by the scale parameter of the wavelet a and by the translation parameter b . The
26 normalization factor $1/a^p$ preserves the energy of the original mother wavelet (for $p=1$). A
27 general description of wavelet methodology can be found in Torrence and Compo (1998). For

1 example, the Mexican-Hat mother wavelet works well with detection of single events, for
2 example in the analysis of coherent structures of ejections and sweeps from a closed-canopy
3 forest (Steiner et al., 2011). On the other hand, the complex Morlet function wavelet is suited
4 to analysis of variance spectrum (Thomas and Foken, 2007). Nordbo and Katul (2013) looked
5 at periodicities of long-term CO₂ fluxes from soil. They showed that the intrinsic smoothing
6 property of the wavelet produces results that are more easily interpretable, without the need
7 of excessive manipulation of the original signal (e.g. averaging, smoothing, and tapering) or
8 without restrictive assumptions (e.g. periodicity, stationarity).

9 The CWT method has an advantage over FFT in that it does not require homogeneity or
10 stationarity, and can reconstruct the time domain to provide specific information on where in
11 space/time and on which frequency the flux occurs. The wavelet flux method allows for the
12 reconstruction of both the frequency and time domains of the flux within a straight stretch of
13 the desired length, and therefore can produce “instantaneous” or “discrete” fluxes which can
14 be directly compared with model estimates. From the pragmatic point of view, calculation of
15 an entire flight segment (e.g. of 100 km) results in not just a single flux value but delivers
16 spatially resolved fluxes at discrete intervals sometimes informally referred to as
17 instantaneous fluxes. Considering the footprint and wavelet scaling parameters, it is possible
18 for an aircraft flying low at approximately 60 m s⁻¹ to provide meaningful spatial flux
19 representation at the 1-2 km resolution (note that the flux calculation was done on ~2 orders
20 of magnitude longer segment) needed for investigating landscape heterogeneity in high
21 resolution biogenic emission models, although in principle even shorter intervals could also
22 be resolved. We determined that for a sufficiently long stretch (e.g. 20-200 km) it is possible
23 to achieve statistically significant discrete wavelet fluxes, on the order of hundreds of meters.
24 To comply with the range of conditions and to ensure statistical significance for the given
25 surface patchiness, the 2 km flux is not just a single value but it is an aggregate of individual
26 wavelet flux values averaged to 2 km. These 2-km fluxes make it flexible to further average
27 spatially to reduce random error related to high variability at short time scales (see Sect. 2.7),
28 before comparing observations with model emissions. An average of the wavelet fluxes can
29 be compared to the Fourier flux from the same stretch. Given the independent approaches, the
30 agreement between the methods adds to the confidence of the flux estimates and the ratio can
31 be used as an additional measure of data quality. Finally the co-spectra from the two methods
32 can be compared. If no high-frequency attenuation losses exist, the co-spectra should be

1 similar. The wavelet approach can also be used for the correction of the FFT high-frequency
2 spectral attenuation if it is related to tubing effects or factors other than the instrument
3 response (Nordbo and Katul, 2013). Here, as the mother wavelet we used the Morlet wavelet.
4 More detailed methodology of wavelet analysis used in this work has been presented by Karl
5 et al. (2013) which was a further development from Karl et al. (2009). Vertical flux
6 divergence of isoprene is expected to be primarily controlled by its relatively short lifetime
7 and was measured directly using “racetracks” at multiple altitudes (Karl et al., 2013). It was
8 found to be similarly linear above different oak ecosystems and heterogeneity. We estimated
9 the contribution of the storage term to the isoprene flux divergence to be of the order of 2-
10 5%, negligibly small compared to sensible heat fluxes. Fluxes were generally measured by
11 flying consistently at 400 m \pm 50 m (a.g.l.) altitude, which was chosen so that the resulting
12 blending length and flux footprint match the spatial scale of surface patchiness (Mahrt, 2000;
13 Raupach and Finnigan, 1995; Wood and Mason, 1991; Mason, 1988). The flux at the aircraft
14 altitude was typically in the range of 5% to 30% smaller than the surface flux depending on
15 the ratio of aircraft altitude to PBL height (z/z_i), and the determined flux divergence linear
16 coefficients were assumed to be relatively constant based on the range of OH concentration
17 estimates for the entire flight track. An alternative method expected to work with similar
18 accuracy would be to use inverse models (Bange et al., 2006). The wavelet coefficients were
19 optimized for the CWT analysis to perform well on stretches between 15 and 200 km with a
20 typical ratio of FFT single flux value to CWT instantaneous flux average of between 1.0 and
21 1.3.

22 2.6.4 Flux footprints

23 The footprint for each flux point was derived using the Weil and Horst (1992) approach and
24 depends on the wind speed, relative altitude to the PBL height, and the convective velocity
25 scale.

26 Here we use scaling developed for the mixed layer according to:

$$27 \quad dx_{0.5} = 0.9 \frac{u \cdot z_m^{2/3} \cdot h^{1/3}}{w^*}, \quad (6)$$

28 where $dx_{0.5}$ is the half width of the horizontal footprint, u the horizontal windspeed, z_m the
29 height above ground, h the PBL height and w^* the convective velocity scale which is derived
30 from the wavelet heat flux in each transect.

1 The source contribution area can be approximated by projecting an upwind-pointed half
2 dome with the $dx_{0.5}$ parameter representing a radius of that half dome (see Supplementary
3 Fig. S5).

4 **2.7 Error analysis (quality of fluxes)**

5 As with eddy covariance on the ground, AEC fluxes must undergo a rigorous quality
6 assessment, if not more so. The total uncertainty in reported airborne flux for a typical flight
7 segment (> 20 km) is the summation of errors from calculation of concentrations (10% for
8 calibrated compounds [5% standard accuracy+5% dilution system], 30% from relative lab-
9 based sensitivity-relative transmission approach), survey-flight-specific random (5% for the
10 typical leg), systematic (1%) errors related to relative altitude within the PBL and to the
11 aircraft leg, random error related to disjunct measurement (less than 1%), error due to storage
12 term (2%) and error due to variability in flux divergence coefficients ($\sim 2\%$, explained further
13 below). For reactive tracers which require divergence corrections to yield the surface flux,
14 uncertainty in PBL estimation (interpolated from saw-tooth soundings) is ± 100 m which
15 translates to 10% of up to 30% of the divergence correction, thus $\sim 3\%$. We estimate the total
16 accuracy for the reported surface fluxes averaged for long segments (e.g. 100 km) to be 20%
17 for calibrated compounds and 40% for other compounds and a typical isoprene flux detection
18 limit of $0.01 \text{ mg m}^{-2} \text{ h}^{-1}$.

19 The vertical flux divergence is dependent on the rate of isoprene oxidation (which depends
20 mostly on OH concentration during daytime), the time rate of change of isoprene
21 concentration (relevant for conserved species), and differential horizontal advection of
22 isoprene with height (small). Based on directly measured flux divergence in the racetrack
23 gradient flights (Karl et al., 2013) we showed clear linear dependence of the flux divergence
24 with a theoretical concentration gradient (e.g. 1.4×10^{-4} ppbv m^{-1} over a homogenous oak
25 terrain and an OH concentration of 6.6×10^6 molec/ cm^3). Since the flux divergence for
26 isoprene was shown to be primarily controlled by OH concentrations (of which we have a
27 range of estimates), we make an informed assumption here that the divergence coefficients
28 we used to scale the fluxes to the surface are accurate within a factor of two for the entire
29 campaign. Thus a change in the flux divergence coefficients by a factor of two could result in
30 only a $\sim 2\%$ difference to the scaled surface flux for a typical z/z_i ratio of 0.3 which is minor
31 relative to other error sources as discussed above. As the correction of the fluxes for flux

1 divergence was typically less than 20%, the contribution from less accurate divergence
2 coefficients is assumed to be relatively minor (up to ~2%) for isoprene but could still be more
3 important for other gases (e.g. CO₂), for which more detailed characterization of flux
4 divergence might be needed in future measurements.

5 The uncertainty of the instantaneous CWT fluxes aggregated to 2-km is dominated by the
6 random error which must be necessarily larger than that for the average flux for the whole leg
7 and is related to high temporal and spatial variability (e.g. Mann and Lenschow, 1994). Using
8 equation 3 from Karl et al. (2013) this error can be of the order of 40-50% but declines with
9 averaging of the 2-km points and is already below 30% when averaging more than 5 km. For
10 this reason we have only evaluated fluxes over longer stretches (>> 2 km). The 2-km
11 representations can provide more flexibility for averaging, for example, individual points can
12 be useful for a regression of isoprene flux versus LAI for all of the 2-km data providing
13 excellent statistics. However, it makes sense to use spatially averaged data (e.g. regional
14 zones) for comparison with the models. While the footprint averaged data are not shown here,
15 such data would be additionally associated with the error related to footprint accuracy which
16 is related to uncertainty in short-term convective scale velocity, PBL height and any
17 variability in wind speed. Thus, the total uncertainty of the surface fluxes of isoprene is
18 estimated at approximately 50% for individual 2-km data points, but at 20% for averages
19 exceeding 10 km.

20 The calibrated concentration data filtered for interferences (e.g. a biomass burning episode;
21 see supplementary video) were used with corrected vertical wind speed data to derive
22 covariance functions for each eligible stretch. The segments were selected for flux calculation
23 based on minimal roll angle of the aircraft between turns, and on consistency of altitude,
24 excluding maneuvers with significant altitude changes such as soundings (see example in
25 Supplementary Fig. S2). Of segments prescreened for validity, only those with a clear peak in
26 the covariance function (Figure 2a) within the lag-time window of 5 s were accepted. The
27 segment data were subsequently examined for similarities in the variances of concentration
28 and vertical wind speed (Figure 2b) together with the time series of wavelet frequency co-
29 spectra (Figure 2c) within the cone of influence (COI) which is the region where the end of
30 the power spectrum may be impacted by edge effects. Rather than excluding the part falling
31 outside the COI, each of the ends of the time series are padded with zeros and excluded
32 afterward, so the results are not affected by the COI. By comparing the wavelet co-spectra

1 with average cross-covariance (Figure 2d) it is possible to determine where in the wavelet
2 period (inverse of frequency) the flux contribution occurs, enabling for example the
3 visualization of the updrafts associated with high emissions.

4 Each stretch was finally analyzed for spectral characteristics, independently for the FFT and
5 CWT methods (see Figure 3). Identical procedures were applied to the fast temperature
6 sensor for comparison. As the co-spectra and ogives demonstrate, the VOC sampling system
7 was not limited by high frequency attenuation owing to the short 0.1 s dwell time and small
8 number of preselected VOCs in the quadrupole mass spectrometer cycle. It was found that
9 the majority of the flux contribution (~90%) was occurring between between 0.1 and 0.01 Hz
10 which translates to the spatial scales of 0.6 to 6 km.

11 Additional quality measures were the ratio of the FFT and CWT fluxes (Figure 4, upper
12 panel), which for isoprene were usually $1 \pm 15\%$ for survey transect flights. Identical values
13 from the two methods were not expected as the FFT flux is affected by nonstationarities and
14 inhomogeneities in contrast to the CWT flux, but the generally good agreement adds
15 confidence to the results. Occasionally, a ratio higher than 1.15 was seen on short segments,
16 or over a nonhomogeneous transect, or when the fluxes were close to zero. In sporadic cases
17 when the fluxes were strongly non-stationary (characterized by the ratio higher than 1.3), the
18 FFT flux was tagged as rejected and the CWT flux was only accepted if all the other quality
19 criteria were fulfilled.

20 The generally good quality of fluxes in CABERNET was due to a combination of factors
21 such as instrument sensitivities, response times, slow aircraft speeds and proximity to the
22 source by flying at low altitudes (e.g. 400 m) and finally lack of spectral interferences (e.g.
23 from propellers). Figure 4 (lower panel) shows the application of flux divergence (only
24 reactive compounds such as isoprene) coefficients from racetrack profiling to derive the
25 surface fluxes from the aircraft fluxes. In the remainder of the manuscript when discussing
26 fluxes, we focus exclusively on the CWT fluxes due to the much higher spatial resolution of
27 the flux and also because of their higher accuracy in cases with inhomogeneity and non-
28 stationarity.

1 2.7.1 Simultaneous ground based measurements

2 Ground based measurements coinciding with aircraft passes in time and space were
3 performed at two sites: The 525-m tall Hearst-Argyle Tower in Walnut Grove, California
4 (WGC) located in the San Joaquin Delta region (38.2636, -121.4899, elevation 1 m) and the
5 23-m tall Tonzi Ranch Tower (TRT) (38.4308, -120.9656, elevation 177 m) located in the
6 relatively homogenous oak forest savannah between the Sierra Nevada foothills and the San
7 Joaquin Delta. Description of these measurements is provided in Supplementary Information.

8

9 **3 Results and discussion**

10 **3.1 Observed Concentrations of BVOC from PTR-MS**

11 The spatial distributions of VOC concentrations measured on most research flights are shown
12 in Figure 5. We show and discuss in this section the individual compounds measured in
13 CABERNET in terms of their concentrations.

14 3.1.1 Isoprene

15 Isoprene concentrations were low, typically less than 50 ppt ($0.05 \text{ mg m}^{-2} \text{ h}^{-1}$ in fluxes) in the
16 Central Valley over agricultural terrains and over urban areas but were very high over the oak
17 woodlands which cover approximately 7% of California, and were the focus of the
18 CABERNET campaign flight plans. In general, observed isoprene concentrations over oak
19 woodlands ranged from less than 1 ppb on cool days up to several ppb on warmer flights. A
20 maximum of 8 ppb was observed on the hottest day. The aircraft also saw marked increases
21 of isoprene near some highways with eucalyptus trees planted alongside. Although no study
22 of regional scale emissions of VOC in California was previously conducted, the pattern of
23 concentrations observed during CABERNET is consistent with an expected pattern based on
24 extrapolation of earlier studies from enclosures of dominant plant species of California which
25 suggested oaks (mostly blue oaks), and to some degree eucalyptus trees, to be likely the most
26 important isoprene emitters in California (e.g. Karlik and Winer, 2001). The broad range of
27 temperatures encountered in different flights (mean range 21 – 33 °C) was responsible for
28 quantitative differences in concentrations over the overlapping segments. The actual
29 concentration at the surface is expected to be significantly higher than observed at aircraft

1 height, as is shown to be the case when flying near the tall tower at Walnut Grove where the
2 top levels (394 and 525 m) saw very tiny concentration of isoprene consistent with the
3 concentrations seen by aircraft although the lowest tower levels (10 and 131 m) saw much
4 higher concentrations (Supplementary Fig. S3b). However, the areas with significant
5 biogenic emissions of isoprene covered a relatively small fetch within the footprint of the
6 Walnut Grove tower.

7

8 3.1.2 Monoterpenes

9 Measurements of monoterpenes from aircraft are subject to several challenges which include
10 1) relatively small source strength, for example, ~10% relative to isoprene measured over
11 coniferous regions; 2) relatively lower PTR-MS sensitivity compared to lighter compounds
12 when using a quadrupole MS; 3) relatively shorter atmospheric lifetimes for some
13 monoterpenes. The majority of the CABERNET aircraft tracks focused on isoprene emitters
14 (e.g. oak woodlands) and not monoterpene emitters (e.g. coniferous forests), so the
15 monoterpene signals were small and therefore we have not attempted to derive fluxes.
16 However, averaging concentration signals to a 0.5 km resolution along the flight path was
17 sufficient to decrease detection limits for monoterpenes to a few ppt and to demonstrate the
18 presence of emissions from the densely forested areas, for instance, on a track towards
19 Blodgett forest and on parts of the mixed conifer habitats along Coastal Ranges. Very high
20 concentrations of monoterpenes exceeding 300 ppt were found in the GC cartridges on the
21 flight legs passing near the Mojave Desert scrublands but m/z 81 and 137 were not included
22 in ions measured by the PTR-MS on that flight.

23 3.1.3 Other VOCs

24 Although we focus on isoprenoids, the aircraft PTR-MS system also measured concentrations
25 (and fluxes) of other compounds with non-biogenic or partially biogenic sources such as
26 dairies (methanol), isoprene photochemistry (MVK+MACR, hydroxyacetone), MBO to
27 exclude interferences with isoprene, and sporadically other compounds such as acetaldehyde
28 or aromatics. The data for these compounds are available and will be reported in other
29 publications.

1 3.1.4 Comparison with Walnut Grove Tower

2 The Twin Otter flew close to the tower on RF2 and RF4 (13:18). The ground-airborne
3 comparison was focused on methanol, isoprene, and MVK+MAC. Overall, the comparison
4 for methanol suggested agreement within 30%. However, looking at simultaneous fine
5 resolution data from the two PTR-MS instruments (Supplementary Fig. S3a), a dip in
6 methanol concentration was seen consistently by both the aircraft and the tower when the
7 plane was closest to the tower's top level, with excellent measurement agreement (11.6 ± 1.16
8 ppbv seen by the tower at 525 m vs 11.9 ± 1.19 ppbv measured by the aircraft at 513 m). The
9 variability of the methanol concentration over a five minute segment adjacent to the tower
10 was within several ppbv, giving insight into spatial variability of methanol at that time and
11 altitude. The WGC region is mostly agricultural with a variety of sparsely distributed trees.
12 The measurement during the aircraft pass at 13:18 showed very little isoprene (below 50 ppt)
13 at the top level of the tower (as mentioned in 3.1.1, and Supplementary Fig. S3b) even though
14 concentrations close to 1 ppb were observed at the 10 m level. The agreement for
15 MVK+MAC (0.18 ± 0.02 ppbv aircraft vs 0.20 ± 0.02 ppbv 525 m tower) was also good.

16

17 3.2 Observed fluxes

18 Isoprene and methanol showed the strongest fluxes of all measured compounds. In this paper
19 we focus on reporting isoprene surface fluxes.

20 3.2.1 Isoprene fluxes

21 The observed surface emission rates of isoprene over oak woodlands ranged from around 1 to
22 $15 \text{ mg m}^{-2} \text{ h}^{-1}$. The measured isoprene flux distribution shown in Figure 6 (CWT fluxes, 2 km
23 resolution) visually confirms earlier predictions that isoprene emissions are almost
24 exclusively produced by oak with a limited contribution from eucalyptus trees. For example,
25 when entering the Sierra Nevada foothill oak band isoprene emissions rose remarkably above
26 the low background in the Central Valley. Karlik and McKay (2002) used an isoprene
27 emission factor from branch enclosure for blue oak of $27 \text{ } \mu\text{g g}^{-1} \text{ h}^{-1}$, and leaf areas and
28 weights from 14 blue oak trees from Sierra Nevada to estimate a leaf-level emission factor of
29 $\sim 8 \text{ mg m}^{-2}(\text{leaf}) \text{ h}^{-1}$, corresponding to a landscape emission factor of $\sim 4 \text{ mg m}^{-2}(\text{land}) \text{ h}^{-1}$ for a
30 setting where oaks occupied half of the land surface area. In CABERNET the airborne

1 emission factors for isoprene over oak woodlands varied from less than 1 to $\sim 10 \text{ mg m}^{-2} \text{ h}^{-1}$
2 with the average EF comprising all the flights over areas with oak presence ($\geq 20\%$ coverage
3 of oak species according to GAP database) of $1.8 \text{ mg m}^{-2} \text{ h}^{-1}$. However, the woodlands varied
4 in species homogeneity, and more significantly, in the fraction (i.e., sparseness and
5 patchiness) of tree coverage. It is necessary to emphasize that while the LAI of oak covered
6 land surfaces has a relatively small range, about 3 to $6 \text{ m}^2 \text{ m}^{-2}$, the fraction of the land surface
7 covered by oaks can range from < 0.1 to 1. For example, Karlik and McKay (2002) using a
8 precise method of calculating the areas of leaves from 14 trees divided by the areas of their
9 crowns, measured an LAI of $4.3 \text{ m}^2 \text{ m}^{-2}$ for oak crown areas but the oaks only covered 42%
10 of the land surface resulting in an area average LAI of $1.8 \text{ m}^2 \text{ m}^{-2}$. For the more sparse
11 terrains the LAI can often be lower than $1 \text{ m}^2 \text{ m}^{-2}$. Compared with the forests with closed
12 canopies, modeling emissions from oak woodlands in California can be regarded as a specific
13 case to which assessment by airborne flux measurements are particularly applicable.
14 Measured airborne emissions reflect the true emissions from these California ecosystems of
15 variable LAI ranging from less than 1 to about $5 \text{ m}^2 \text{ m}^{-2}$.

16

17 3.2.2 Comparison of isoprene fluxes at Tonzi Ranch Tower

18 The aircraft flew over the Tonzi Ranch Tower twice, allowing two snapshot comparisons
19 between the airborne CWT and ground based REA flux measurements. It is important to note
20 that the airborne CWT averages over ~ 0.5 minute (2 km), while the ground based REA
21 averages over 30 minutes, and that the footprints related to each measurement are necessarily
22 quite different, likely do not have the same oak biomass density, and thus the comparison is
23 not expected to be perfect. In the first instance, the half-hourly REA flux was in excellent
24 agreement with the 2-km average wavelet surface flux over the tower (i.e. $0.12 \pm 0.06 \text{ mg m}^{-2}$
25 h^{-1} REA vs $0.12 \pm 0.06 \text{ mg m}^{-2} \text{ h}^{-1}$ aircraft) while on the returning flight the ground based flux
26 was 1/3 of the aircraft flux (i.e. $0.26 \pm 0.13 \text{ mg m}^{-2} \text{ h}^{-1}$ REA vs $0.87 \pm 0.44 \text{ mg m}^{-2} \text{ h}^{-1}$).
27 Interestingly, the next half-hour REA flux was $0.96 \pm 0.48 \text{ mg m}^{-2} \text{ h}^{-1}$, much closer to the
28 aircraft value. This may be due to a shift in wind direction and variability in oak biomass
29 density around the tower but it should also be noted that the uncertainty in a single REA flux
30 measurement is high and individual values are typically averaged to improve accuracy.
31 These comparisons obviously suffer from significant uncertainties due to different footprints

1 at different altitudes, different temporal coverage, and even temperature/PAR homogeneities.
2 Nevertheless, the comparison provides insight about the variability in measurements at
3 different scales, confirms observations at these scales are in a similar range, and indicates
4 how airplane and tower measurements are complementary. A larger period of overlap in a
5 future campaign is needed for gaining better statistics on such comparisons.

6 3.2.3 Comparison of isoprene emission factors to MEGAN landcover 2.2

7 Isoprene emission model estimates are based on basal emission rates, landcover
8 characteristics, and the changes in emission associated with the environmental parameters
9 temperature and photosynthetically active radiation (PAR). The airborne surface flux
10 normalized for temperature and radiation using the Guenther et al. (2006) activity factor can
11 be used to derive airborne basal emission factors (BEFs) to directly compare to emission
12 factors used by models (e.g. the MEGAN emission factors version 2.2). A spatial comparison
13 is shown in Figure 6. It needs to be noted that such an approach introduces additional
14 uncertainty from the temperature and PAR datasets and the algorithm used for calculating the
15 activity coefficient, which are much higher than the uncertainty of the measured surface
16 fluxes because of high sensitivity to errors in temperature and PAR. For this reason, in this
17 manuscript we treat this comparison as semi-quantitative, and will explore this in more detail
18 as part of another paper (Misztal et al., 2014) which focuses on using the airborne data to
19 examine the accuracy of several different BVOC emission models, including detailed
20 sensitivity analyses and input data validation. However, the qualitative picture clearly shows
21 the remarkable correspondence of airborne BEFs derived at 2 km spatial resolution with
22 landcover BEFs at a similar resolution. The transition from the low emitting environment in
23 the Central Valley to highly emitting areas occupied by oak woodlands is clear (as shown
24 earlier in Figure 1). The most accurate match can be seen, for example, in the central part of
25 the Sierra foothills and on the southern Coastal Range, to the south east of Monterey Bay and
26 in the oak savannas near San Francisco Bay (Orinda, and Diablo Valley). The BEFs decline
27 to zero over water bodies (e.g. San Francisco Bay, or lakes on the central-northern Sierras).
28 There are some areas which do not agree well, for example, in the north-east over the Sierras
29 which are dominated by conifers where airborne BEFs were somewhat lower. On the other
30 hand, the areas where aircraft showed higher BEFs (e.g. beginning of RF8) are most likely
31 related to inaccuracies in the oak landcover database.

1

2 **4 Conclusions**

3 We successfully made airborne eddy covariance flux measurements and mapped out
4 horizontally varying source distributions of isoprene emissions for the dominant oak emitting
5 ecosystems in California. The extensive oak woodlands in California are the most important
6 regional source of isoprene which may be particularly relevant for air quality near heavily
7 polluted regions of Central Valley. We observed high concentrations (up to 8 ppbv) and high
8 surface emissions of isoprene ranging from several to more than ten $\text{mg m}^{-2} \text{h}^{-1}$ from the oak
9 woodlands in the foothills of the Sierra Nevada and Coastal Ranges. Consistent with other
10 studies we show that in the Central Valley isoprene emissions are typically undetectably
11 small at aircraft level except for the areas of Eucalyptus trees planted near the highways. The
12 temperature ranges in California cause changes in the isoprene emissions from relatively low
13 to extremely high due to their strong temperature sensitivity. The ability of CWT for
14 calculating fluxes at high spatial resolution (e.g. 2 km averaging) provides an optimal data set
15 to compare BEFs from measurements with models. The data from this study will be used to
16 assess isoprene emission-factor databases and isoprene emission response to landcover
17 characteristics predicted for BVOC emission models. In the future, the ability to measure
18 direct airborne fluxes over heterogeneous landscapes should be useful to improve landcover
19 descriptions in biogenic emission models, characterize flux for the entire VOC spectrum by
20 PTR-MS equipped with a Time-of-Flight detector, and potentially for cross-calibration of
21 data from satellite-column retrievals.

22 **Acknowledgements**

23 We gratefully acknowledge California Air Resources Board (CARB) for funding
24 CABERNET Contract #09-339, and the CIRPAS team for help in instrument integration. We
25 acknowledge Abhinav Guha (UC Berkeley) for his contributions to the successful campaign.
26 Finally, we would like to thank Andrew Turnipseed (NCAR) and Tiffany Duhl (NCAR) for
27 performing GC analyses of aircraft cartridges, and Steve Shertz (NCAR) for engineering
28 support. NCAR is sponsored by the National Science Foundation. Alex Guenther was partly
29 funded under the Laboratory Directed Research and Development Program at PNNL, a multi-
30 program national laboratory operated by Battelle for the U.S. Department of Energy under
31 Contract DE-AC05-76RL01830. We also acknowledge Prof. Maggi Kelly at GIF, UC

- 1 Berkeley for suggestions regarding geospatial landcovers. We thank Jeremy Avise and Klaus
- 2 Scott at California Air Resources Board for collaboration and useful modeling suggestions.
- 3

1 **References**

- 2 Apel, E., Riemer, D., Hills, A., Baugh, W., Orlando, J., Faloona, I., Tan, D., Brune, W.,
3 Lamb, B., and Westberg, H.: Measurement and interpretation of isoprene fluxes and isoprene,
4 methacrolein, and methyl vinyl ketone mixing ratios at the PROPHET site during the 1998
5 Intensive, *Journal of Geophysical Research*, 107, 4034, 2002.
- 6 Arey, J., Corchnoy, S. B., and Atkinson, R.: Emission of linalool from Valencia orange
7 blossoms and its observation in ambient air, *Atmos Environ a-Gen*, 25, 1377-1381, 1991.
- 8 Arey, J., Crowley, D. E., Crowley, M., Resketo, M., and Lester, J.: Hydrocarbon Emissions
9 from Natural Vegetation in California South-Coast-Air-Basin, *Atmospheric Environment*, 29,
10 2977-2988, Doi 10.1016/1352-2310(95)00137-N, 1995.
- 11 Baker, B., Guenther, A., Greenberg, J., Goldstein, A., and Fall, R.: Canopy fluxes of 2-
12 methyl-3-buten-2-ol over a ponderosa pine forest by relaxed eddy accumulation: Field data
13 and model comparison, *J Geophys Res-Atmos*, 104, 26107-26114, Doi
14 10.1029/1999jd900749, 1999.
- 15 Baldocchi, D. D.: Assessing the eddy covariance technique for evaluating carbon dioxide
16 exchange rates of ecosystems: past, present and future, *Global Change Biol*, 9, 479-492,
17 2003.
- 18 Bange, J., Zittel, P., Spiess, T., Uhlenbrock, J., and Beyrich, F.: A new method for the
19 determination of area-averaged turbulent surface fluxes from low-level flights using inverse
20 models, *Boundary-Layer Meteorology*, 119, 527-561, DOI 10.1007/s10546-005-9040-6,
21 2006.
- 22 Claussen, M.: Area-Averaging of Surface Fluxes in a Neutrally Stratified, Horizontally
23 Inhomogeneous Atmospheric Boundary-Layer, *Atmos Environ a-Gen*, 24, 1349-1360, Doi
24 10.1016/0960-1686(90)90041-K, 1990.
- 25 Desjardins, R. L., Hart, R. L., Macpherson, J. I., Schuepp, P. H., and Verma, S. B.: Aircraft-
26 Based and Tower-Based Fluxes of Carbon-Dioxide, Latent, and Sensible Heat, *J Geophys
27 Res-Atmos*, 97, 18477-18485, 1992.
- 28 Fares, S., Gentner, D. R., Park, J. H., Ormeno, E., Karlik, J., and Goldstein, A. H.: Biogenic
29 emissions from Citrus species in California, *Atmospheric Environment*, 45, 4557-4568, DOI
30 10.1016/j.atmosenv.2011.05.066, 2011.
- 31 Fares, S., Park, J. H., Gentner, D. R., Weber, R., Ormeno, E., Karlik, J., and Goldstein, A. H.:
32 Seasonal cycles of biogenic volatile organic compound fluxes and concentrations in a
33 California citrus orchard, *Atmos Chem Phys*, 12, 9865-9880, DOI 10.5194/acp-12-9865-
34 2012, 2012.
- 35 Fuentes, J. D., and Wang, D.: On the seasonality of isoprene emissions from a mixed
36 temperate forest, *Ecological Applications*, 9, 1118-1131, Doi 10.2307/2641382, 1999.
- 37 Goldstein, A., Hultman, N., Fracheboud, J., Bauer, M., Panek, J., Xu, M., Qi, Y., Guenther,
38 A., and Baugh, W.: Effects of climate variability on the carbon dioxide, water, and sensible
39 heat fluxes above a ponderosa pine plantation in the Sierra Nevada (CA), *Agr Forest
40 Meteorol*, 101, 113-129, 2000.

1 Goldstein, A. H., Goulden, M. L., Munger, J. W., Wofsy, S. C., and Geron, C. D.: Seasonal
2 course of isoprene emissions from a midlatitude deciduous forest, *Journal of Geophysical*
3 *Research: Atmospheres* (1984–2012), 103, 31045-31056, 1998.

4 Goldstein, A. H., and Schade, G. W.: Quantifying biogenic and anthropogenic contributions
5 to acetone mixing ratios in a rural environment, *Atmospheric Environment*, 34, 4997-5006,
6 Doi 10.1016/S1352-2310(00)00321-6, 2000.

7 Guenther, A., Karl, T., Harley, P., Wiedinmyer, C., Palmer, P. I., and Geron, C.: Estimates of
8 global terrestrial isoprene emissions using MEGAN (Model of Emissions of Gases and
9 Aerosols from Nature), *Atmos. Chem. Phys.*, 6, 3181-3210, 10.5194/acp-6-3181-2006, 2006.

10 Guenther, A. B., Jiang, X., Heald, C. L., Sakulyanontvittaya, T., Duhl, T., Emmons, L. K.,
11 and Wang, X.: The Model of Emissions of Gases and Aerosols from Nature version 2.1
12 (MEGAN2.1): an extended and updated framework for modeling biogenic emissions, *Geosci*
13 *Model Dev*, 5, 1471-1492, DOI 10.5194/gmd-5-1471-2012, 2012.

14 Hegg, D. A., Covert, D. S., Jonsson, H., and Covert, P. A.: Determination of the transmission
15 efficiency of an aircraft aerosol inlet, *Aerosol Sci Tech*, 39, 966-971, Doi
16 10.1080/02786820500377814, 2005.

17 Karl, T., Guenther, A., Turnipseed, A., Patton, E. G., and Jardine, K.: Chemical sensing of
18 plant stress at the ecosystem scale, *Biogeosciences*, 5, 1287-1294, 2008.

19 Karl, T., Apel, E., Hodzic, A., Riemer, D. D., Blake, D. R., and Wiedinmyer, C.: Emissions
20 of volatile organic compounds inferred from airborne flux measurements over a megacity,
21 *Atmos Chem Phys*, 9, 271-285, 2009.

22 Karl, T., Misztal, P. K., Jonsson, H. H., Shertz, S., Goldstein, A. H., and Guenther, A. B.:
23 Airborne Flux Measurements of BVOCs above Californian Oak Forests: Experimental
24 Investigation of Surface and Entrainment Fluxes, OH Densities, and Damkohler Numbers, *J*
25 *Atmos Sci*, 70, 3277-3287, Doi 10.1175/Jas-D-13-054.1, 2013.

26 Karl, T. G., Spirig, C., Rinne, J., Stroud, C., Prevost, P., Greenberg, J., Fall, R., and
27 Guenther, A.: Virtual disjunct eddy covariance measurements of organic compound fluxes
28 from a subalpine forest using proton transfer reaction mass spectrometry, *Atmos Chem Phys*,
29 2, 279-291, 2002.

30 Karlik, J. F., and Winer, A. M.: Measured isoprene emission rates of plants in California
31 landscapes: comparison to estimates from taxonomic relationships, *Atmospheric*
32 *Environment*, 35, 1123-1131, 2001.

33 Karlik, J. F., and McKay, A. H.: Leaf area index, leaf mass density, and allometric
34 relationships derived from harvest of blue oaks in a California oak savanna, USDA Forest
35 Service General Technical Report Number PSW-GTR-184, Albany, CA, 2002.

36 Kristensen, L., Mann, J., Oncley, S. P., and Wyngaard, J. C.: How close is close enough
37 when measuring scalar fluxes with displaced sensors?, *J Atmos Ocean Tech*, 14, 814-821,
38 Doi 10.1175/1520-0426(1997)014<0814:Hcicew>2.0.Co;2, 1997.

39 Kuhn, U., Rottenberger, S., Biesenthal, T., Wolf, A., Schebeske, G., Ciccioli, P., Brancaleoni,
40 E., Frattoni, M., Tavares, T., and Kesselmeier, J.: Isoprene and monoterpene emissions of
41 Amazonian tree species during the wet season: Direct and indirect investigations on
42 controlling environmental functions, *Journal of Geophysical Research*, 107, 8071, 2002.

1 Kurpius, M. R., and Goldstein, A. H.: Gas-phase chemistry dominates O₃ loss to a forest,
2 implying a source of aerosols and hydroxyl radicals to the atmosphere, *Geophys Res Lett*, 30,
3 Artn 1371
4 Doi 10.1029/2002gl016785, 2003.

5 Lamb, B., Westberg, H., and Allwine, G.: Isoprene Emission Fluxes Determined by an
6 Atmospheric Tracer Technique, *Atmospheric Environment*, 20, 1-8, Doi 10.1016/0004-
7 6981(86)90201-5, 1986.

8 Langford, B., Misztal, P. K., Nemitz, E., Davison, B., Helfter, C., Pugh, T. A. M.,
9 MacKenzie, A. R., Lim, S. F., and Hewitt, C. N.: Fluxes and concentrations of volatile
10 organic compounds from a South-East Asian tropical rainforest, *Atmos. Chem. Phys.*, 10,
11 8391-8412, 10.5194/acp-10-8391-2010, 2010.

12 Lenschow, D. H., Delany, A. C., Stankov, B. B., and Stedman, D. H.: Airborne
13 Measurements of the Vertical Flux of Ozone in the Boundary-Layer, *Boundary-Layer*
14 *Meteorology*, 19, 249-265, Doi 10.1007/Bf00117223, 1980.

15 Lenschow, D. H., Pearson, R., and Stankov, B. B.: Estimating the Ozone Budget in the
16 Boundary-Layer by Use of Aircraft Measurements of Ozone Eddy Flux and Mean
17 Concentration, *J Geophys Res-Oc Atm*, 86, 7291-7297, 1981.

18 Lenschow, D. H.: Probing the Atmospheric Boundary Layer, *Probing the Atmospheric*
19 *Boundary Layer*, American Meteorological Society, Boston, MA, 1986.

20 Loreto, F., and Sharkey, T. D.: A gas-exchange study of photosynthesis and isoprene
21 emission in *Quercus rubra* L, *Planta*, 182, 523-531, 1990.

22 Mahrt, L.: Surface heterogeneity and vertical structure of the boundary layer, *Boundary-*
23 *Layer Meteorology*, 96, 33-62, Doi 10.1023/A:1002482332477, 2000.

24 Mann, J., and Lenschow, D. H.: Errors in Airborne Flux Measurements, *J Geophys Res-*
25 *Atmos*, 99, 14519-14526, Doi 10.1029/94jd00737, 1994.

26 Mason, P. J.: The Formation of Areally-Averaged Roughness Lengths, *Q J Roy Meteor Soc*,
27 114, 399-420, DOI 10.1002/qj.49711448007, 1988.

28 Mauder, M., Desjardins, R. L., and MacPherson, I.: Scale analysis of airborne flux
29 measurements over heterogeneous terrain in a boreal ecosystem, *J Geophys Res-Atmos*, 112,
30 Artn D13112
31 Doi 10.1029/2006jd008133, 2007.

32 Metzger, S., Junkermann, W., Mauder, M., Butterbach-Bahl, K., Trancón y Widemann, B.,
33 Neidl, F., Schäfer, K., Wieneke, S., Zheng, X., and Schmid, H.: Spatially explicit
34 regionalization of airborne flux measurements using environmental response functions,
35 *Biogeosciences*, 10, 2193-2217, 2013.

36 Misztal, P. K., Avise, J., Karl, T., Scott, K., Weber, R., Jonsson, H. H., Guenther, A. B., and
37 Goldstein, A. H.: Evaluation of regional isoprene emission estimates in California based on
38 direct airborne flux measurements, In preparation for ACP, 2014.

39 Moore, C.: Frequency response corrections for eddy correlation systems, *Boundary-Layer*
40 *Meteorology*, 37, 17-35, 1986.

- 1 Nordbo, A., and Katul, G.: A Wavelet-Based Correction Method for Eddy-Covariance High-
2 Frequency Losses in Scalar Concentration Measurements, *Boundary-Layer Meteorology*,
3 146, 81-102, 10.1007/s10546-012-9759-9, 2013.
- 4 Panofsky, H. A., and Dutton, J. A.: *Atmospheric turbulence: models and methods for*
5 *engineering applications*, Wiley, New York, 1984.
- 6 Park, J.-H., Goldstein, A. H., Timkovsky, J., Fares, S., Weber, R., Karlik, J., and Holzinger,
7 R.: Active Atmosphere-Ecosystem Exchange of the Vast Majority of Detected Volatile
8 Organic Compounds, *Science*, 341, 643-647, 10.1126/science.1235053, 2013.
- 9 Pattey, E., Strachan, I., Desjardins, R., and Massheder, J.: Measuring nighttime CO₂ flux
10 over terrestrial ecosystems using eddy covariance and nocturnal boundary layer methods, *Agr*
11 *Forest Meteorol*, 113, 145-158, 2002.
- 12 Pierce, T., Geron, C., Bender, L., Dennis, R., Tonnesen, G., and Guenther, A.: Influence of
13 increased isoprene emissions on regional ozone modeling, *J Geophys Res-Atmos*, 103,
14 25611-25629, Doi 10.1029/98jd01804, 1998.
- 15 Rasmussen, R. A.: Isoprene: Identified as a forest-type emission to the atmosphere,
16 *Environmental Science & Technology*, 4, 667-671, 1970.
- 17 Raupach, M. R., and Finnigan, J. J.: Scale Issues in Boundary-Layer Meteorology - Surface-
18 Energy Balances in Heterogeneous Terrain, *Hydrol Process*, 9, 589-612, DOI
19 10.1002/hyp.3360090509, 1995.
- 20 Reid, J. S., Jonsson, H. H., Smith, M. H., and Smirnov, A.: Evolution of the vertical profile
21 and flux of large sea-salt particles in a coastal zone, *J Geophys Res-Atmos*, 106, 12039-
22 12053, Doi 10.1029/2000jd900848, 2001.
- 23 Rinne, H., Guenther, A., Greenberg, J., and Harley, P.: Isoprene and monoterpene fluxes
24 measured above Amazonian rainforest and their dependence on light and temperature,
25 *Atmospheric Environment*, 36, 2421-2426, 2002.
- 26 Rowe, M. D., Fairall, C. W., and Perlinger, J. A.: Chemical sensor resolution requirements
27 for near-surface measurements of turbulent fluxes, *Atmos. Chem. Phys.*, 11, 5263-5275,
28 10.5194/acp-11-5263-2011, 2011.
- 29 Schade, G. W., Goldstein, A. H., and Lamanna, M. S.: Are monoterpene emissions
30 influenced by humidity?, *Geophys Res Lett*, 26, 2187-2190, Doi 10.1029/1999gl900444,
31 1999.
- 32 Schade, G. W., Goldstein, A. H., Gray, D. W., and Lerda, M. T.: Canopy and leaf level 2-
33 methyl-3-buten-2-ol fluxes from a ponderosa pine plantation, *Atmospheric Environment*, 34,
34 3535-3544, Doi 10.1016/S1352-2310(00)00120-5, 2000.
- 35 Schade, G. W., and Goldstein, A. H.: Fluxes of oxygenated volatile organic compounds from
36 a ponderosa pine plantation, *J Geophys Res-Atmos*, 106, 3111-3123, Doi
37 10.1029/2000jd900592, 2001.
- 38 Scott, K. I., and Benjamin, M. T.: Development of a biogenic volatile organic compounds
39 emission inventory for the SCOS97-NARSTO domain, *Atmospheric Environment*, 37, S39-
40 S49, Doi 10.1016/S1352-2310(03)00381-9, 2003.
- 41 Serca, D., Guenther, A., Klinger, L., Vierling, L., Harley, P., Druilhet, A., Greenberg, J.,
42 Baker, B., Baugh, W., Bouka-Biona, C., and Loemba-Ndembu, J.: EXPRESSO flux

1 measurements at upland and lowland Congo tropical forest site, *Tellus B*, 53, 220-234, DOI
2 10.1034/j.1600-0889.2001.01237.x, 2001.

3 Sharkey, T. D., Singsaas, E. L., Lerdau, M. T., and Geron, C. D.: Weather effects on isoprene
4 emission capacity and applications in emissions algorithms, *Ecological Applications*, 9,
5 1132-1137, 1999.

6 Steiner, A., Pressley, S., Botros, A., Jones, E., Chung, S., and Edburg, S.: Analysis of
7 coherent structures and atmosphere-canopy coupling strength during the CABINEX field
8 campaign, *Atmos Chem Phys*, 11, 11921-11936, 2011.

9 Stoy, P. C., Richardson, A. D., Baldocchi, D. D., Katul, G. G., Stanovick, J., Mahecha, M.
10 D., Reichstein, M., Detto, M., Law, B. E., Wohlfahrt, G., Arriga, N., Campos, J.,
11 McCaughey, J. H., Montagnani, L., Paw U, K. T., Sevanto, S., and Williams, M.: Biosphere-
12 atmosphere exchange of CO₂ in relation to climate: a cross-biome analysis across multiple
13 time scales, *Biogeosciences*, 6, 2297-2312, 10.5194/bg-6-2297-2009, 2009.

14 Thomas, C., and Foken, T.: Detection of long-term coherent exchange over spruce forest
15 using wavelet analysis, *Theor Appl Climatol*, 80, 91-104, 2005.

16 Thomas, C., and Foken, T.: Flux contribution of coherent structures and its implications for
17 the exchange of energy and matter in a tall spruce canopy, *Boundary-Layer Meteorology*,
18 123, 317-337, DOI 10.1007/s10546-006-9144-7, 2007.

19 Torrence, C., and Compo, G. P.: A practical guide to wavelet analysis, *B Am Meteorol Soc*,
20 79, 61-78, 1998.

21 Vargas, R., Detto, M., Baldocchi, D. D., and Allen, M. F.: Multiscale analysis of temporal
22 variability of soil CO₂ production as influenced by weather and vegetation, *Global Change*
23 *Biol*, 16, 1589-1605, 2010.

24 Weil, J. C., and Horst, T. W.: Footprint Estimates for Atmospheric Flux Measurements in the
25 Convective Boundary-Layer, *Precipitation Scavenging and Atmosphere-Surface Exchange*,
26 Vols 1-3, 717-728, 1992.

27 Westberg, H., Lamb, B., Hafer, R., Hills, A., Shepson, P., and Vogel, C.: Measurement of
28 isoprene fluxes at the PROPHET site, *Journal of Geophysical Research: Atmospheres* (1984–
29 2012), 106, 24347-24358, 2001.

30 Winer, A. M., Arey, J., Atkinson, R., Aschmann, S. M., Long, W. D., Morrison, C. L., and
31 Olszyk, D. M.: Emission Rates of Organics from Vegetation in California Central Valley,
32 *Atmos Environ a-Gen*, 26, 2647-2659, Doi 10.1016/0960-1686(92)90116-3, 1992.

33 Wood, N., and Mason, P.: The Influence of Static Stability on the Effective Roughness
34 Lengths for Momentum and Heat-Transfer, *Q J Roy Meteor Soc*, 117, 1025-1056, DOI
35 10.1002/qj.49711750108, 1991.

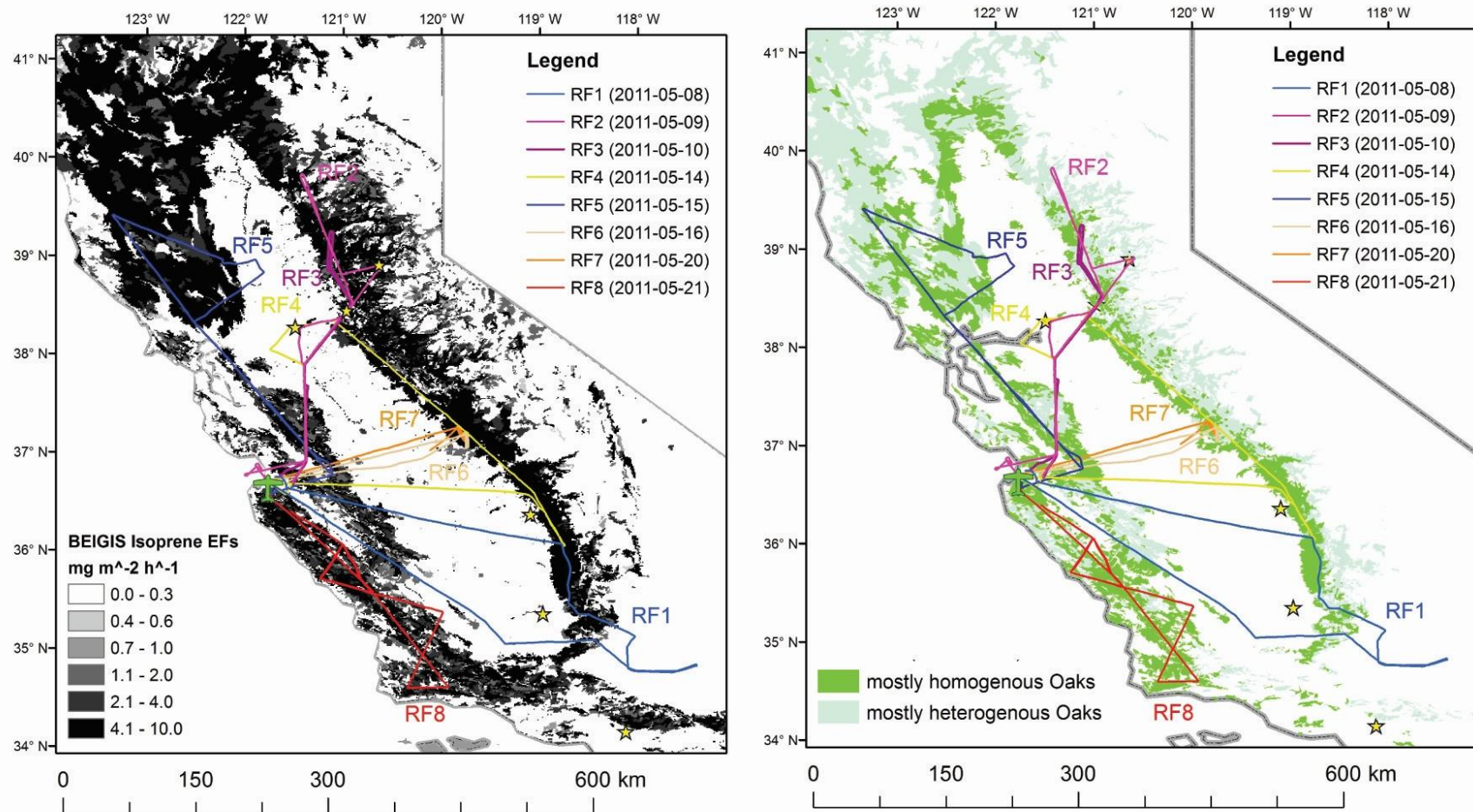
36 Wyngaard, J. C., and Brost, R. A.: Top-down and bottom-up diffusion of a scalar in the
37 convective boundary layer, *J Atmos Sci*, 41, 102-112, 1984.

38

1 Table 1. Selected flight parameter data specific to each research flight

| | RF1 June 8 | RF2 June 9 | RF3 June 10 | RF4 June 14 | RF5 June 15 | RF6 June 16 | RF7 June 20 | RF8 June 21 |
|---|---------------------------|-------------------------------|----------------------|-------------------------------|-------------------------------|------------------|------------------|---------------------------|
| Temperature close to the surface (2 m WRF) (°C) | | | | | | | | |
| mean | 20.6 | 23.1 | 24.4 | 27.8 | 28.5 | 24.8 | 29.7 | 32.5 |
| (median) | (21.5) | (23.8) | (25.3) | (28.6) | (29.4) | (25.4) | (30.3) | (33.4) |
| s.d. | 3.21 | 3.21 | 3.46 | 2.88 | 3.24 | 3.96 | 2.64 | 3.54 |
| min | 11.3 | 10.9 | 11.4 | 11.7 | 12.2 | 11.8 | 12.1 | 11.7 |
| max | 25.9 | 28.0 | 29.6 | 32.1 | 33.8 | 31.4 | 34.9 | 37.2 |
| 5 th percentile | 14.4 | 17.1 | 17.7 | 23.4 | 22.6 | 16.8 | 26.0 | 27.0 |
| 95 th percentile | 24.6 | 27.1 | 28.5 | 31.1 | 32.3 | 29.6 | 32.4 | 36.0 |
| Altitude (m a.g.l.) | | | | | | | | |
| mean | 603 | 551 | 831 | 529 | 511 | 836 | 852 | 462 |
| (median) | (437) | (449) | (685) | (470) | (489) | (721) | (730) | (396) |
| s.d. | 436 | 309 | 575 | 233 | 193 | 461 | 565 | 210 |
| min | 127 | 119 | 126 | 209 | 127 | 55.3 | 50.0 | 160 |
| max | 2410 | 1830 | 2790 | 1720 | 1460 | 2610 | 1870 | 1540 |
| 5 th percentile | 251 | 266 | 285 | 301 | 278 | 291 | 289 | 268 |
| 95 th percentile | 1670 | 1300 | 2090 | 949 | 712 | 1640 | 1830 | 887 |
| Convective velocity scale ^a , w^* (m/s) | | | | | | | | |
| mean | 4.40 | 3.56 | 3.19 | 3.20 | 2.61 | 3.62 | 3.42 | 2.86 |
| (median) | (4.42) | (3.46) | (2.94) | (3.21) | (2.47) | (3.61) | (3.43) | (2.62) |
| s.d. | 1.55 | 0.92 | 1.19 | 1.01 | 0.79 | 1.12 | 0.85 | 1.11 |
| min | 1.18 | 1.64 | 1.27 | 1.18 | 0.84 | 1.72 | 2.2 | 1.12 |
| max | 8.25 | 8.69 | 8.13 | 5.72 | 5.11 | 6.25 | 4.95 | 5.87 |
| 5 th percentile | 1.87 | 2.22 | 1.54 | 1.62 | 1.46 | 1.99 | 2.31 | 1.33 |
| 95 th percentile | 7.01 | 5.12 | 5.25 | 4.67 | 4.10 | 5.58 | 4.82 | 4.99 |
| Other flight characteristics | | | | | | | | |
| Take off time UTC (local/PDT) | 17:30 (11:30) | 18:15 (12:15) | 18:10 (12:10) | 18:05 (12:05) | 18:00 (12:00) | 19:05 (13:05) | 19:05 (13:05) | 18:55 (12:55) |
| Touchdown time UTC (local/PDT) | 22:20 (16:20) | 22:45 (16:45) | 22:10 (16:10) | 22:35 (16:35) | 22:30 (16:30) | 0:05 (18:05) | 00:30 (18:30) | 23:30 (17:30) |
| Flight focus | Survey | Survey | Survey, Racetrack | Survey | Survey | Racetrack | Racetrack | Survey |
| Total length (km) | 983 | 908 | 802 | 896 | 875 | 1020 | 835 | 935 |
| PBL height range (km) | 0.9 - 2.8 | 1.4 - 1.7 | 0.8-1.1 | 0.4-1.9 | 1.1-1.1 | 1.6-1.7 | 1.2-1.2 | 0.7-1.4 |
| VOC-related m/z measured (10 Hz) ^b | 69, 33, 79, 93, 107 | 69, 71, 33, 81, 137, 87 | 69, 71, 75, 33 | 69, 71, 33, 81, 137, 87 | 69, 71, 33, 81, 137, 45 | 69, 71, 87 | 69, 71, 75 | 69, 71, 33, 137, 87 |

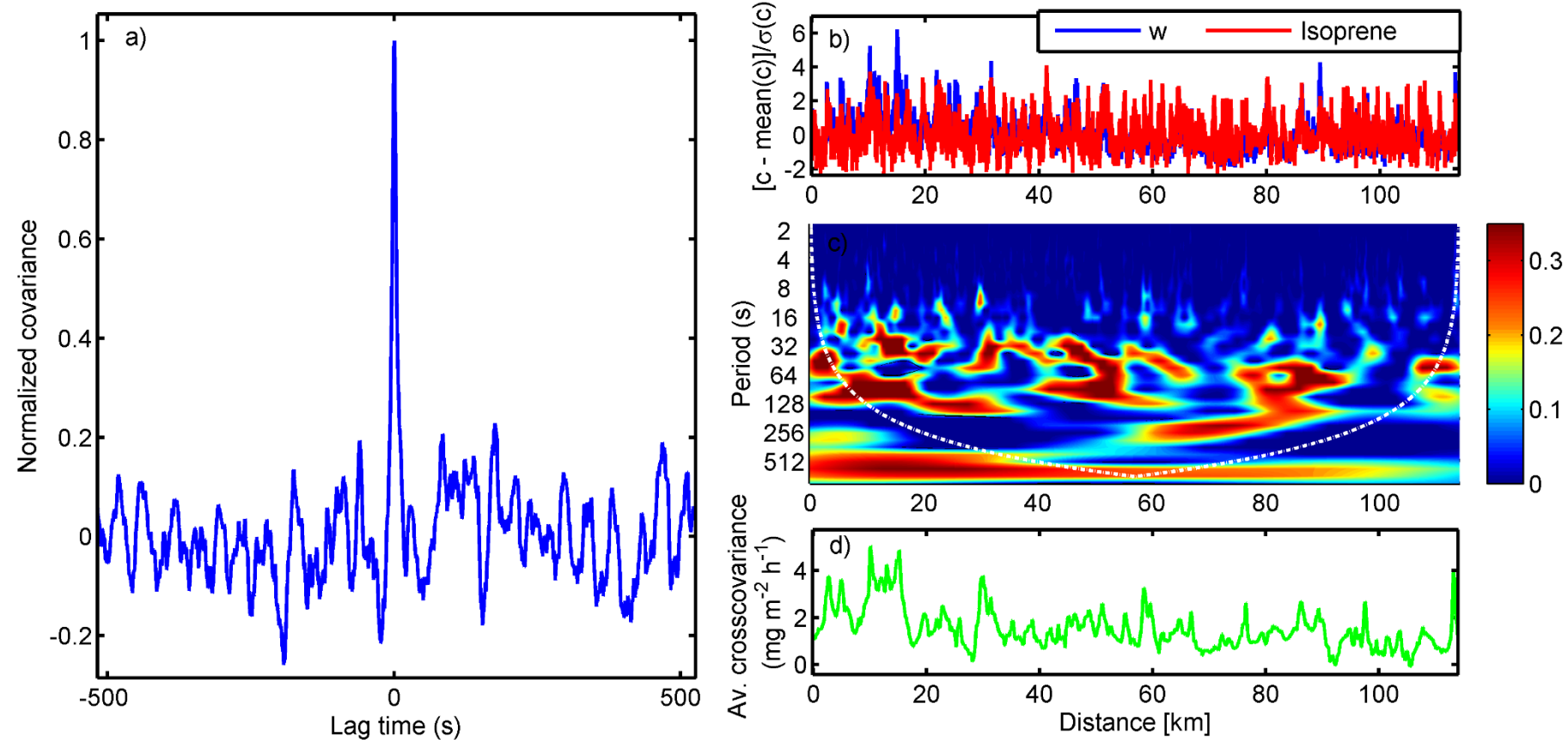
2 ^aapproximated from wavelet heat fluxes (uncorrected) on survey tracks (including only the lowest racetrack levels);
^b m/z 21, 32, and 37 were also measured on every flight at 10, 20 and 20 Hz respectively.



1

2 Figure 1. Tracks flown during CABERNET overlaid over (a) BEIGIS Isoprene Emission Factor (EF) landcover; and (b) oak-woodland ecosystems differing in oak species
 3 spatial homogeneity (according to the GAP database).

1

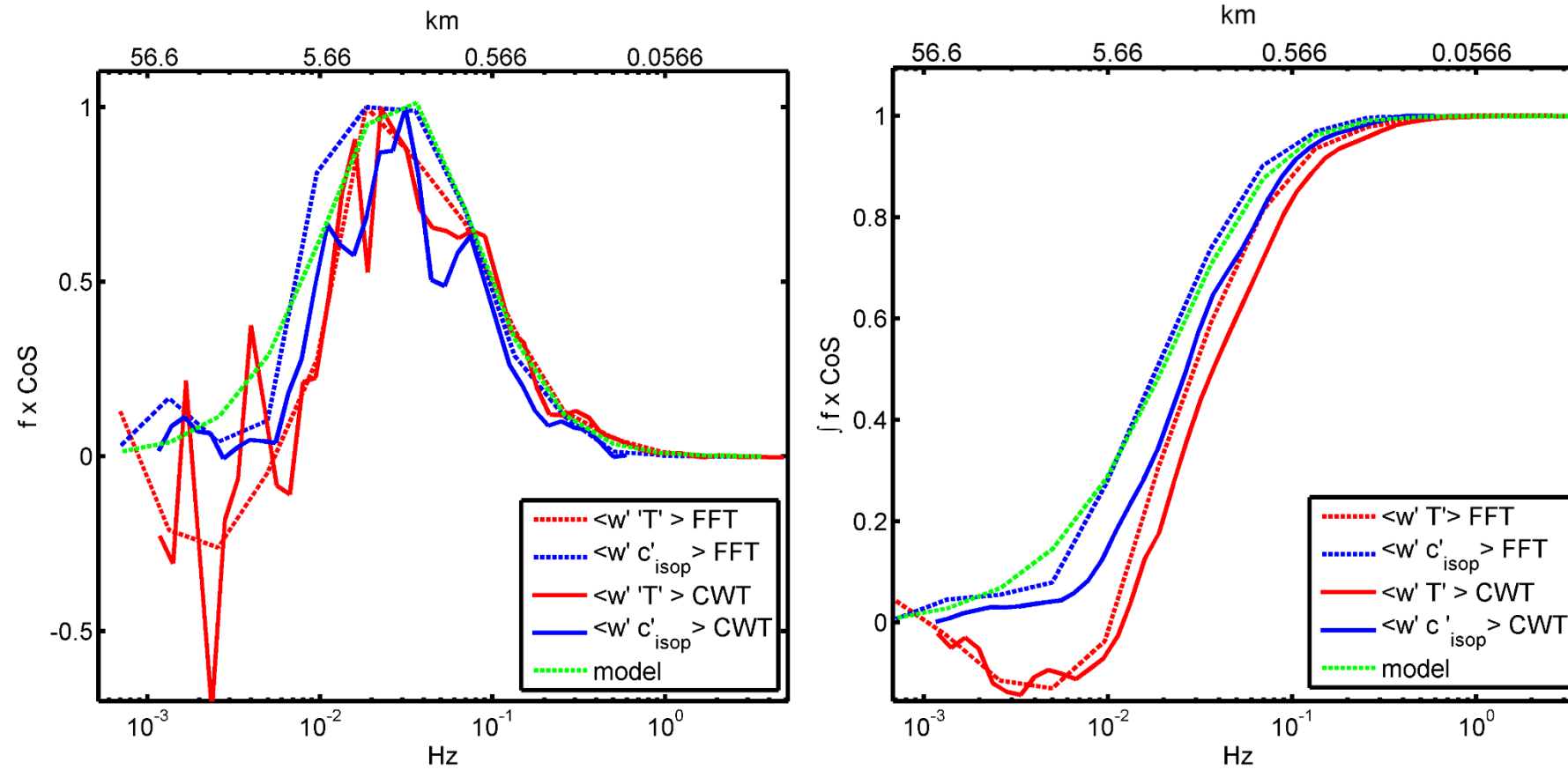


2

3 Figure 2. Flux quality control for an example flight leg (the segment from Supplementary Fig. S2). a) Clear peak in the covariance
4 function; b) variances of w and isoprene; c) time-resolved wavelet co-spectra; and d) average cross-variance.

1

2

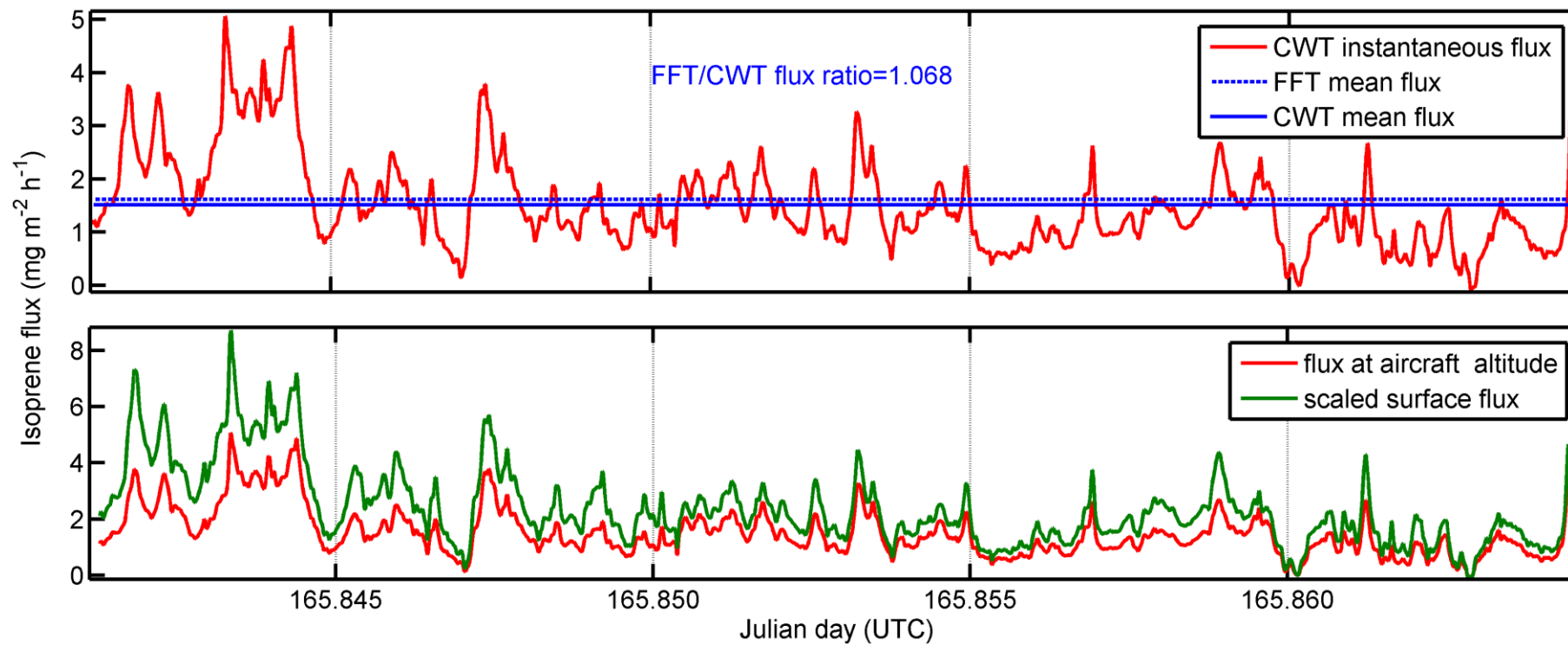


3

4

Figure 3. Spectral quality control of the example flight segment. Left panel: Comparison of co-spectra for isoprene flux and heat flux using the FFT and CWT methods independently; Right panel: Cumulative co-spectra for isoprene flux and heat flux using the FFT and CWT methods independently. The green lines in left and right panels show the model that is used with transfer functions optimized from Kristensen et al. (1997).

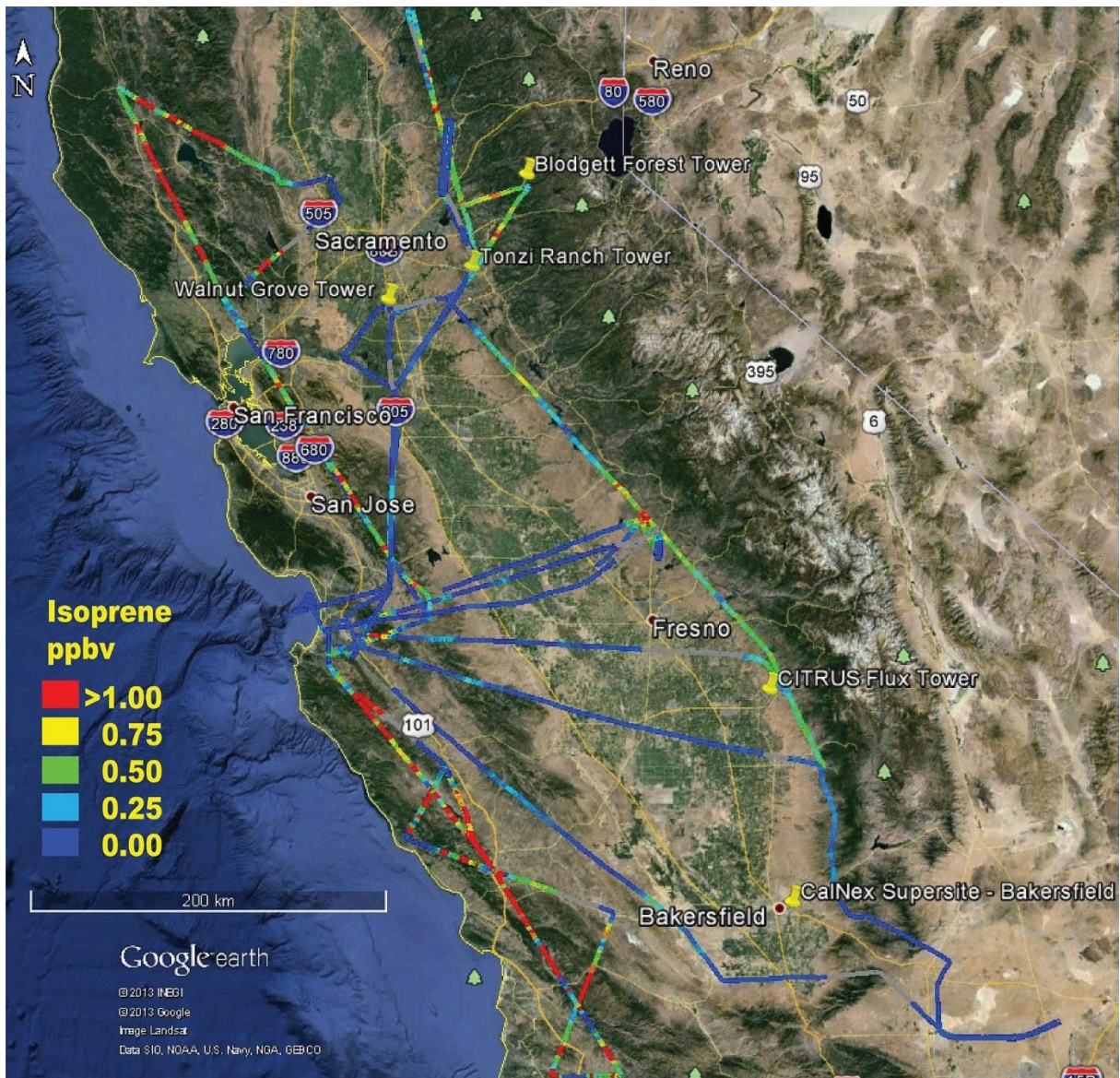
1
2



3
4
5

Figure 4. Isoprene flux processing. Upper panel: determination of the FFT/CWT flux ratio; lower panel: application of flux divergence coefficients (derived in racetrack profiles) to scale fluxes from aircraft altitude to surface fluxes using aircraft altitude and PBL height.

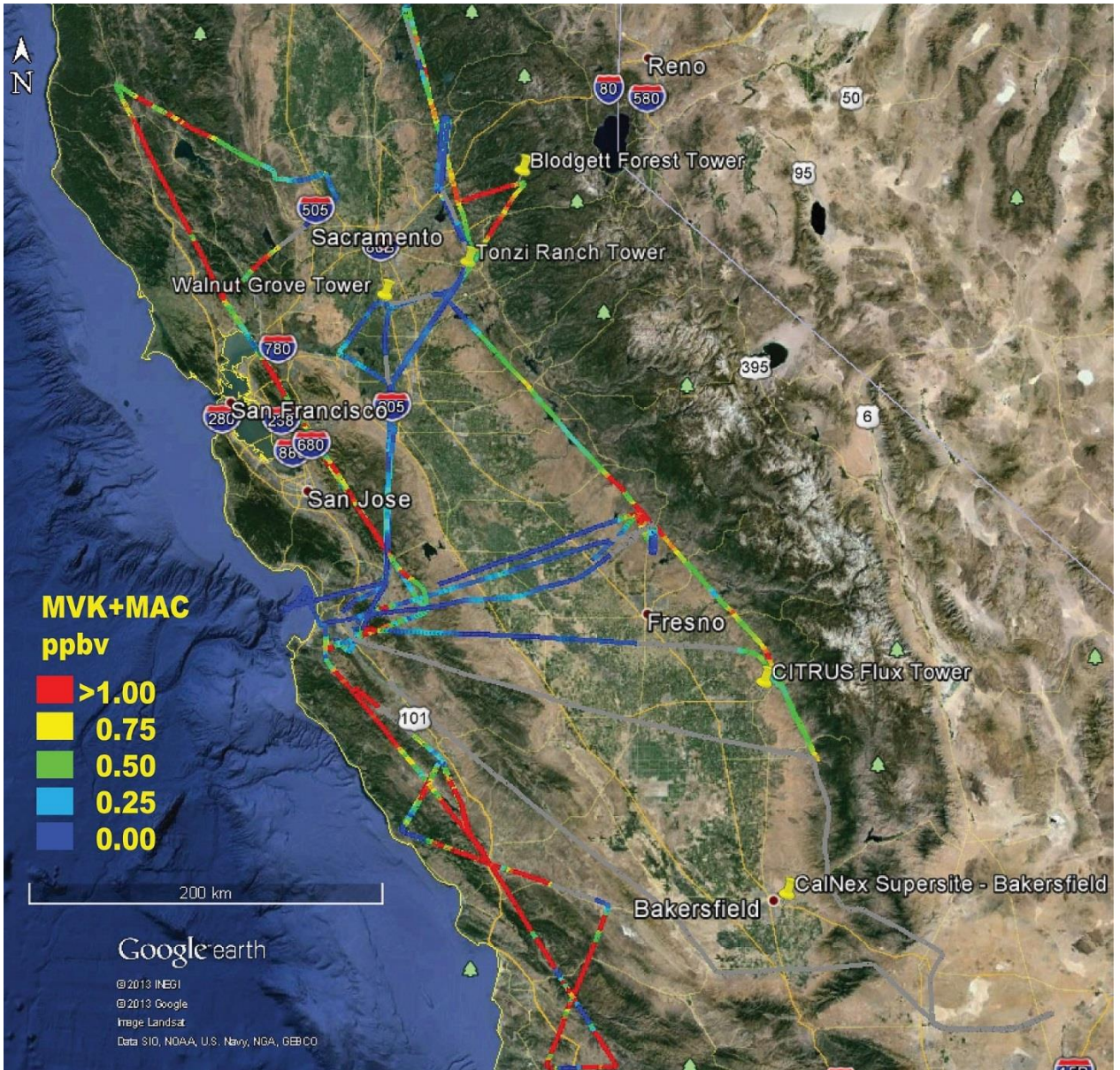
1 a)



2

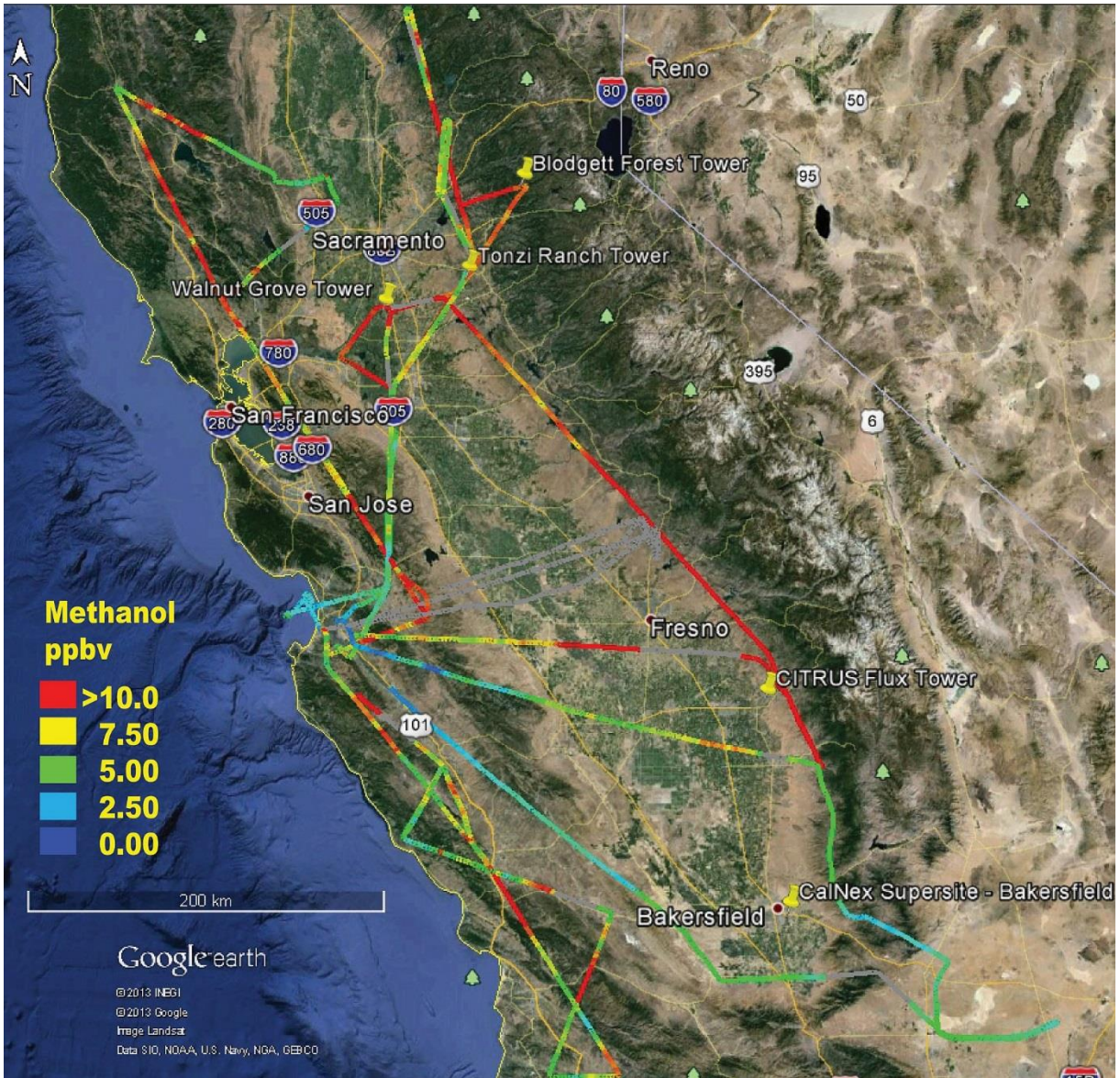
3

1 b)



2
3
4
5
6
7
8
9

1 c)



2

3

4

5

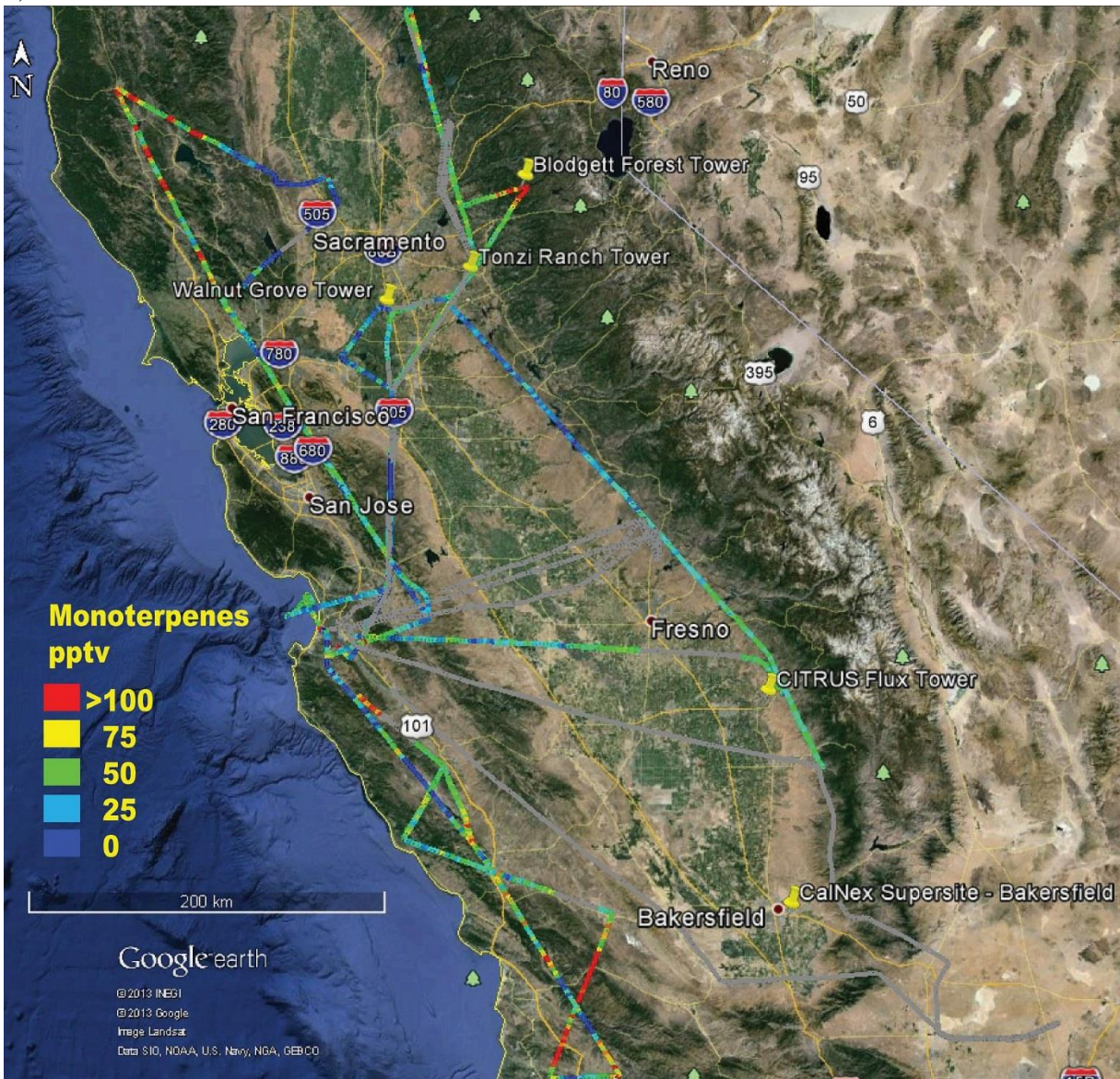
6

7

8

9

1 d)



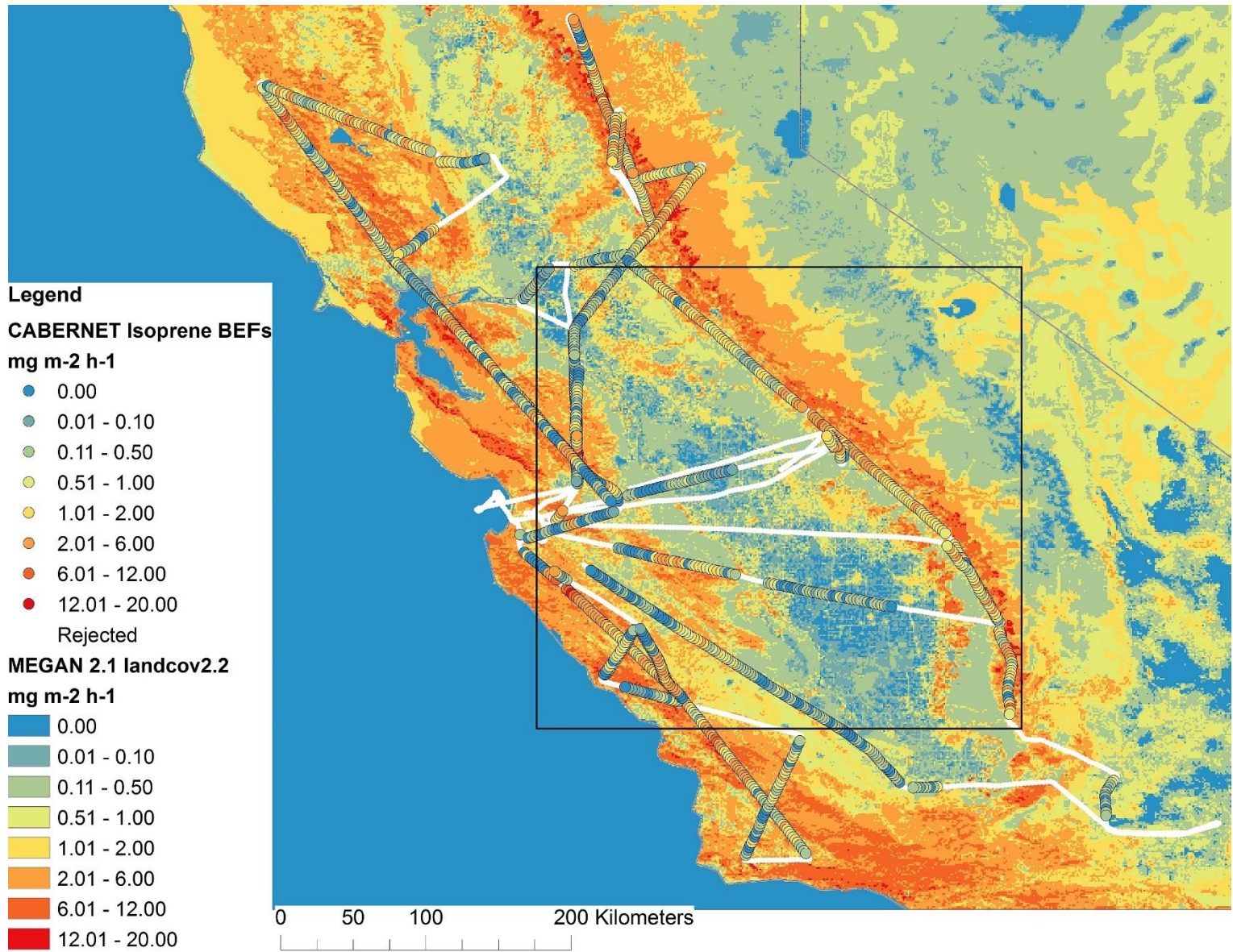
2

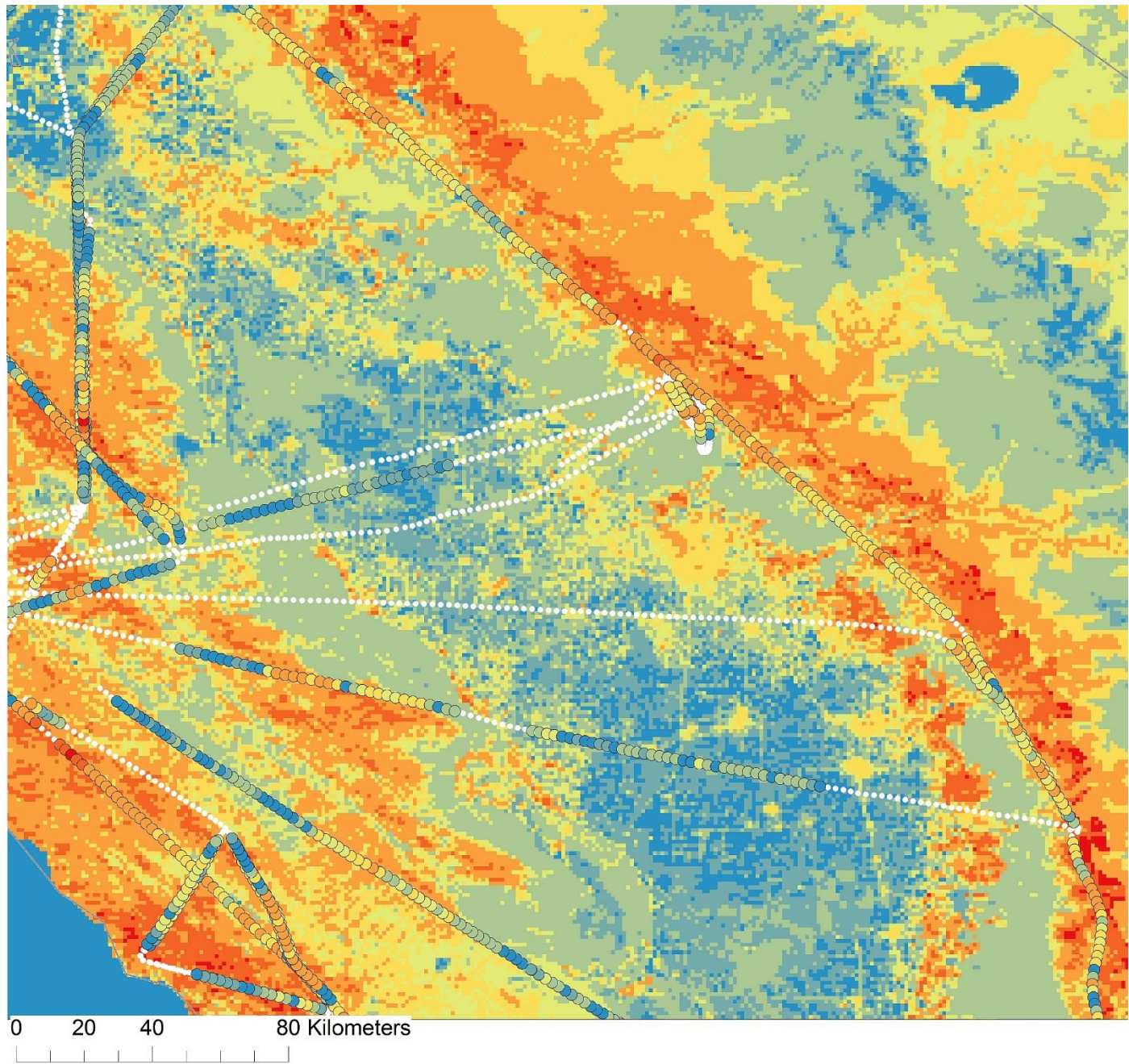
3 Figure 5. Spatial distributions of concentrations of a) isoprene, b) MVK+MAC, c) methanol
4 and d) monoterpenes measured during CABERNET

5

6

7





1

- 1 Figure 6. Comparison of airborne BEFs with MEGAN's landcover 2.2 for isoprene (airborne BEFs are subject to additional uncertainties
- 2 introduced from T, and PAR and the algorithm's activity factor used in normalization).a) full extent with a rectangle denoting b) zoomed area.
- 3